

WATER RESOURCE RESPONSES TO CLIMATE IN THE WATER-ENERGY-FOOD
NEXUS OF THE PAJARO VALLEY WATERSHED, CA

45
36
2019
ERTH
.A48

A Thesis submitted to the faculty of
San Francisco State University
In partial fulfillment of
the requirements for
the Degree

Master of Science

In

Geosciences

by

Deandra Jenelle Alvear

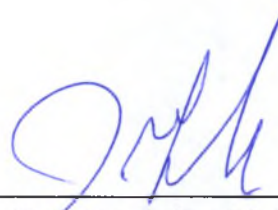
San Francisco, California

May 2019

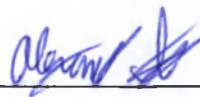
Copyright by
Deandra Jenelle Alvear
2019

CERTIFICATION OF APPROVAL

I certify that I have read WATER RESOURCE RESPONSES TO CLIMATE IN THE WATER-ENERGY-FOOD NEXUS OF THE PAJARO VALLEY WATERSHED, CA by Deandra Jenelle Alvear, and that in my opinion this work meets the criteria for approving a thesis submitted in partial fulfillment of the requirement for the degree Master of Science in Geosciences at San Francisco State University.



Dr. Jason J. Gurdak Ph.D.
Associate Professor



Dr. Alexander Stine Ph.D.
Assistant Professor



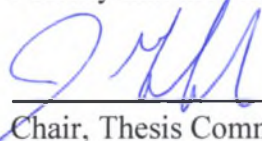
Dr. Piero Mazzini Ph.D.
Assistant Professor

WATER RESOURCE RESPONSES TO CLIMATE IN THE WATER-ENERGY-FOOD
NEXUS OF THE PAJARO VALLEY WATERSHED, CA

Deandra Jenelle Alvear
San Francisco, California
2019

Climate variability and change are major factors that affect groundwater resources on a global scale. However, it is still poorly understood how components of the hydrologic system respond to these signals of climate variability. The crucial role of groundwater in the water-energy-food nexus underscores the need to better understand how climate will affect groundwater in the future. This need is especially urgent in coastal agricultural regions where groundwater is the primary source of water. This thesis quantifies the response of hydrologic processes and human interaction to interannual to multidecadal climate variability in coastal aquifers, specifically the El Niño Southern Oscillation (2-7 year cycle) and Pacific Decadal Oscillation (15-30 year cycle), in Pajaro Valley, California, located in California's coastal aquifer system. I examined whether climate signals were present in long-term records of precipitation, streamflow, groundwater levels, recharge, and pumping using Singular Spectrum Analysis. I quantified the response of these variables to modes of climate variability by performing lag correlations. These analyses illustrate the extent to which the Pajaro Valley watershed responds to climatic and anthropogenic forcings. The findings from my research can aid water managers in creating sustainable groundwater management practices in areas that are highly groundwater dependent and experiencing the negative effects of groundwater overdraft.

I certify that the Abstract is a correct representation of the content of this thesis.



Chair, Thesis Committee

5-21-2019

Date

ACKNOWLEDGEMENTS

I would like to acknowledge and thank my thesis advisor, Dr. Jason Gurdak, for his guidance and encouragement while working on this project. Additionally, I would like to thank my committee members Dr. Alexander Stine and Dr. Piero Mazzini for their insightful questions and comments. I must also acknowledge the financial support I received from the Doris and David Dawdy Hydrology Research Grant and the R-08-Init Project, entitled “Human-Environmental Security in the Asia-pacific Ring of Fire: Water-Energy-Food Nexus” of the Research Institute for Humanity and Nature. I would also like to recognize my fellow graduate students Lawrence Fujiwara, Jessica Rodriguez, Jeremiah Smith, and Cassandra Wolf for their support and friendship throughout this project. I am also eternally grateful to my parents, Rick and Vanessa, for their unwavering support and encouragement that inspired me to pursue this journey.

TABLE OF CONTENTS

List of Tables	ix
List of Figures	xi
List of Appendices.....	xiii
1.0 INTRODUCTION.....	1
2.0 BACKGROUND.....	6
2.1 Climate Variability.....	6
2.2 Climate Variability in the Equatorial Pacific	6
2.2.1 The El Niño Southern Oscillation	6
2.2.2 The Pacific Decadal Oscillation	7
2.3 Study Area.....	8
3.0 METHODOLOGY	10
3.1 Data Selection.....	10
3.2 Time Series Analysis.....	11
3.2.1 Data Pre-Processing.....	12
3.2.2 Singular Spectrum Analysis (SSA)	14
3.2.3 Lag Correlations	17
4.0 RESULTS AND DISCUSSION	18
4.1 Percent Variance of Climate Variability Signals in Hydrologic Time Series	18
4.2 Lag Correlations.....	18
4.2.1 Climate.....	19

TABLE OF CONTENTS (CONT.)

4.2.2 Precipitation	20
4.2.3 Groundwater.....	21
4.3 How does climate affect the water for food relationship within the WEF Nexus of Pajaro Valley?	24
4.4 How does climate influence human interactions in the hydrologic system in terms of groundwater pumping?.....	27
4.5 To what extent does seawater intrusion respond to wet and dry periods?.....	29
5.0 CONCLUSION	32
6.0 REFERENCES.....	34
7.0 TABLES	39
8.0 FIGURES.....	47
9.0 APPENDIX.....	63

LIST OF TABLES

Table	Page
1. Summary of data used in this thesis.....	39
2. The percent variance of reconstructed components (RCs).....	39
3. Results of the climate index to hydrologic inflows lag correlation	40
4. Results of the climate index to hydrologic outflows lag correlation	40
5. Results of the precipitation to hydrologic inflows lag correlation.....	41
6. Results of the hydrologic inflows to outflows lag correlation.....	42
7. Results of the climate index to groundwater levels lag correlation	43
8. Results of hydrologic inflows to groundwater levels lag correlation	44
9. Results of the hydrologic outflows to groundwater levels lag correlation.....	46

LIST OF FIGURES

Figure	Page
1. Timeseries of the MEI and PDO Indices.....	47
2. Map of Pajaro Valley, CA	48
3. Lag correlation plot of climate indices to hydrologic inflows.....	49
4. Lag correlation plot of climate indices to hydrologic outflows.....	50
5. Lag correlation plot of precipitation to hydrologic inflows	51
6. Lag correlation plot of hydrologic inflows to outflows	52
7. Lag correlation plot of climate indices to observed and simulated groundwater levels	53
8. Lag correlation plot of hydrologic inflows to observed groundwater levels.....	54
9. Lag correlation plot of hydrologic inflows to simulated groundwater levels.....	55
10. Lag correlation plot of hydrologic outflows to observed and simulated groundwater levels	56
11. Timeseries of ENSO-composite RCs of precipitation plotted with the MEI Index.....	57
12. Timeseries of ENSO-composite RCs of precipitation and streamflow discharge	57
13. Timeseries of ENSO-composite RCs of precipitation and simulated groundwater recharge.	58
14. Exported ENSO-composite RCs within the precipitation timeseries plotted with phases of strong to moderate El Niño and La Niña events.....	58
15. Exported ENSO-composite RCs within the streamflow discharge timeseries plotted with phases of strong to moderate El Niño and La Niña events	59

LIST OF FIGURES (CONT.)

Figure	Page
16. Exported ENSO-composite RCs within the simulated groundwater recharge timeseries plotted with phases of strong to moderate El Niño and La Niña events	59
17. Timeseries of ENSO-composite simulated groundwater pumping plotted with the MEI Index.	60
18. Exported ENSO-composite RCs of simulated groundwater pumping volume are plotted with phases of strong to moderate El Niño and La Niña events	60
19. (a.) Raw observed groundwater levels and (b.) exported ENSO-composite RCs of observed groundwater levels plotted with phases of strong to moderate El Niño and La Niña events	61
20. (a.) Raw coastal, (b.) raw inland, and (c.) exported ENSO-composite RCs of simulated groundwater levels plotted with phases of strong to moderate El Niño and La Niña events	62

LIST OF APPENDICES

Appendix	Page
A. Results of the Singular Spectrum Analysis	63

1.0 INTRODUCTION

The effect of climate on critical resources such as water, energy, and food has become a global concern not only due to climate change, but to socioeconomic changes such as population growth, urbanization, and the growing demand of natural resources as well. Interannual to multidecadal climate variability has been shown to influence changes in spatiotemporal patterns of various hydrologic processes such as precipitation, streamflow, and surface-water and groundwater storage (Brabets and Walvoord, 2009; Hanson et al., 2006; Kuss and Gurdak, 2014; McCabe et al., 2004). Climate variability can also be linked to the frequency, intensity, and location of extreme climate events such as floods, droughts, and hurricanes (Chikamoto et al., 2015; Higgins et al., 2007). In response to these concerns, the concept of the water-energy-food nexus emerged.

The Water-Energy-Food (WEF) Nexus concept has recently received broad attention in the scientific literature and emerged in the international community as a new sustainable development paradigm (Endo et al., 2015; Hoff, 2011; Leck et al., 2015). The nexus describes the complex relationship between water, energy, and food while also accounting for the linkages, conflicts, and tradeoffs between them. Groundwater is the largest source of accessible freshwater and is crucial in meeting water demands globally, especially in semi-arid and arid regions and during periods of drought when surface-water resources are diminished. This demand for groundwater has led to consequences such as groundwater overdraft, seawater intrusion in coastal areas, groundwater quality degradation, land subsidence and associated infrastructure damage, streamflow depletion,

wetland and ecological damage, loss of springs, and loss of aquifer storage (Famiglietti, 2014; Gurdak, 2017; Konikow and Kendy, 2005). With water as an input to agricultural production within the WEF Nexus, groundwater depletion is a stressor on agricultural regions to meet the demand for food (Smidt et al., 2016). Consequently, many over-drafted aquifers sustain many of the world's most productive agricultural regions (Famiglietti, 2014). Therefore, understanding the complex relations between the WEF Nexus may help stakeholders reduce conflict and tradeoff between water for food in groundwater supported agricultural regions.

The state of California has a \$45 billion agriculture industry that relies on groundwater, which accounts for 30-60% of the state's annual water use. Groundwater is critical to the industry especially during dry years and droughts when surface water is scarce (CDFA, 2016; Liu, 2017). The Central Coast of California makes up a substantial part of the state's agricultural production and is part of the California Coastal aquifer system. In these areas, components of the nexus are significantly limited due characteristics such as large populations, limited freshwater resources, sea level rise and seawater intrusion (Masterson and Garabedian, 2007). To grow food these coastal areas require more water and energy in an area where these resources are already stressed and vulnerable to overdraft, which causes sea water intrusion (Ferguson and Gleeson, 2012; Hanson et al., 2014).

The WEF Nexus in agricultural regions can be described as follows: water is an input to agricultural production (water-food) and is used for cooling at energy generation

facilities (water-energy); energy is necessary to produce, treat, and distribute water (energy-water), as well as power farm machinery (energy-food); and food fuels the labor force required to produce both water (food-water) and energy (food-energy) (Wada et al., 2016). This thesis focuses on the water for food relationship of the nexus, specifically in Pajaro Valley, CA, an agricultural region that has been experiencing seawater intrusion since the 1950s (Hanson et al., 2014), and how long-term climate variability affects groundwater levels of this coastal aquifer. Understanding the relationship between climate and water can better inform sustainable management practices, including conjunctive use of surface-water and groundwater for agriculture and domestic uses, and responding to climate variability (Earman and Dettinger, 2011; Gurdak et al., 2007; Hanson et al., 2006; Holman, 2006; Wada et al., 2010).

This thesis explores the link between climate and water resources by quantifying the relationship between interannual to multidecadal climate oscillations and changes in hydrologic processes that affect surface-water and groundwater resources. Two oscillations originating in the equatorial Pacific Ocean, the El Niño Southern Oscillation (ENSO) and the Pacific Decadal Oscillation (PDO), are linked to shifts in the intensity and timing of weather patterns in the western U.S. (Ropelewski and Halpert, 1986; Sabziparvar et al., 2011; Shang et al., 2011). There is abundant literature that supports how these climate oscillations affects surface hydrologic processes (e.g. Brabets and Walvoord, 2009; Kondrashov et al., 2005; Mazouz et al., 2012), and other studies infer their teleconnections to groundwater levels in areas around the world (Anderson and Emanuel, 2008; Dickinson

et al., 2004; Fleming and Quilty, 2006; Gurdak et al., 2007; Hanson et al., 2006; Holman et al., 2011; Perez-Valdivia et al., 2012; Pool, 2005; Tremblay et al., 2011; Venencio and García, 2011). However, it is still poorly understood how groundwater resources respond to and preserve signals of climate variability on interannual to multidecadal timescales.

To address this knowledge gap, this thesis will quantify how the WEF Nexus that drives seawater intrusion in the Pajaro Valley Watershed, responds to climate variability on interannual to multidecadal timescales. I will explore this by answering the following questions: (1) How does climate affect the water for food relationship within WEF nexus, in Pajaro Valley?; (2) How does climate influence human interactions in the hydrologic system in terms of groundwater pumping?; (3) To what extent does seawater intrusion respond to wet and dry periods? To answer these questions, I will analyze how long-term records of precipitation, streamflow discharge, simulated and observed groundwater levels, simulated recharge and groundwater pumping are interconnected and how well these variables respond to and preserve ENSO and PDO signals. Correlating hydrologic variables to climatic indices are useful in assessing responses to various climatic scenarios (Whittemore et al., 2016). I expect that the hydrologic variables will be strongly correlated to the ENSO and PDO indices due to their teleconnection with the Central Coast of California. I also expect the hydrologic inflows to respond to wet (El Niño) and dry (La Niña) periods accordingly; precipitation, streamflow, and simulated recharge will increase (decrease) during El Niño (La Niña) events. I expect that simulated groundwater pumping will also be well correlated to the climate indices, precipitation, and streamflow discharge;

pumping will increase (decrease) during dry (wet) periods. Farmers will choose to pump less if there is surface water available, which is connected to climatic forcings such as precipitation. Lastly, I anticipate that groundwater levels, observed and simulated, will increase (decrease) during wet (dry) periods. If there is surface water available, demand for groundwater will decrease, allowing the groundwater levels to increase. Conversely, I expect groundwater levels will decrease to levels well below sea level during La Niña years, resulting in sea water intrusion.

Previous studies (Kuss and Gurdak, 2014; Velasco et al., 2015) have examined responses of only the groundwater levels in several principal aquifers to modes of interannual to multidecadal climate variability. In this study, I evaluate the relationship between all parts of the hydrologic system to climate variability and integrate the response of groundwater levels to anthropogenic forcings as well. This research is important due to the location of the Pajaro Valley Watershed, a productive agricultural region, in California's coastal aquifer system. The agricultural demand for groundwater has resulted in groundwater overdraft and seawater intrusion, resulting in conflict and tradeoff among stakeholders of the water-food component of the WEF Nexus. This conflict could lead to further degradation of groundwater and surface water resources and eventually the inability of this area to meet crop demand (Food and Agriculture Organization of the United Nations, 2014). Gaining a deeper understanding of the connections and responses among hydrologic variables and human interactions in this area is important in order to advise water managers to integrate sustainable water practices. Reducing conflict within this local

nexus could help in finding solutions to reduce conflict within the global WEF nexus and prepare for the projected increase in demand for water, energy, and food in the future.

2.0 BACKGROUND

2.1 Climate Variability

Natural climate variability occurs on various temporal and spatial scales and is characterized in terms of anomalies, which are defined as the difference between current climate conditions and the mean state of conditions (Hurrell et al., 2003; Kuss and Gurdak, 2014). Some of these anomalies include changes in the mean distribution of sea level pressure (SLP), the deviation from mean sea-surface temperatures (SSTs), variations in oceanic wind strength, or a combination of multiple variables (Ghil, 2002; Hurrell et al., 2003; NOAA, 2018). Climate indices, such as the Multivariate ENSO Index (MEI) and the Pacific Decadal Oscillation (PDO) Index, are created using a variety of these anomalies at different locations around the globe.

2.2 Climate Variability in the Equatorial Pacific

2.2.1 The El Niño-Southern Oscillation

The El Niño-Southern Oscillation (ENSO) is a system of natural climate variability that occurs irregularly every 2-7 years and is characterized by anomalies in sea surface temperature (SST) and sea level pressure (SLP) in the equatorial Pacific (Hanson et al., 2006; NOAA, 2018). ENSO is considered one of the most important patterns of interannual climate variability due to its high frequency, seasonal effects on weather, and global impact

on average and extreme weather events (Cayan et al., 1999; McCabe and Dettinger, 1999; Ropelewski and Halpert, 1987; Velasco et al., 2015). ENSO has a warm (positive) phase, El Niño, and a cool (negative) phase, La Niña, and the MEI (Figure 1a) is an index made up of the combined El Niño/La Niña phases. The index is based on multiple variables of the Comprehensive Ocean-Atmospheric Data Set (COADS), and represents a weighted average of sea level pressure, zonal and meridional winds, sea surface temperature and total cloudiness in the equatorial Pacific (Wolter and Timlin, 2011). The positive (negative) MEI is related to the positive (negative) ENSO phase (Kuss and Gurdak, 2014; NOAA, 2018). Generally, the Southwestern U.S. experiences above average precipitation during the El Niño phase due to the warm waters of the western Pacific migrating eastward, creating a shift in the jet stream (Higgins et al., 2007; McCabe and Dettinger, 1999; Pool, 2005; Ropelewski and Halpert, 1986; Schonher and Nicholson, 1989). During the La Niña phase, the Southern U.S. experiences drier than normal conditions along with cooler SSTs in the equatorial Pacific (Kiladis and Diaz, 1989; Ropelewski and Halpert, 1986). In the Central Coast of California, the El Niño phase typically results in above average precipitation during winter, and drier conditions during the La Niña phase (Gurdak et al., 2009; Shang et al., 2011).

2.2.2 The Pacific Decadal Oscillation

The Pacific Decadal Oscillation (PDO) is described as a long-lived El Niño-composite pattern of Pacific climate variability on a decadal to interdecadal timescale (Kuss and Gurdak, 2014; Mantua and Hare, 2002; Zhang et al., 1997). The PDO has two

general periodicities of 15-30 years and 50-70 years and is characterized by anomalies in SST and SLP in the North Pacific Ocean. Climate anomalies associated with the PDO are similar to that of the ENSO with comparable shifts in the jet stream (Mantua and Hare, 2002). During the positive (negative) phase of the PDO, SSTs are cooler (warmer) than normal along the coast of California (Mantua and Hare, 2002). During positive PDO there is decreased winter precipitation and sustained droughts in the Northwestern U.S. and wetter than normal conditions in the Southwestern U.S., including southern California; during negative PDO precipitation patterns are reversed (Hanson et al., 2006; Mantua and Hare, 2002; Velasco et al., 2015). Anomalies in climate and oceanic characteristics are used to create the PDO Index (Figure 1b). Shifts in the phase of PDO also affect the phase and occurrence of the ENSO; during the negative (positive) PDO, there is a greater occurrence of the negative (positive) ENSO (Brown and Comrie, 2004; Gutzler et al., 2002; Kuss and Gurdak, 2014). Additionally, the influence of ENSO can be enhanced by the PDO if both oscillations are in the same phase (Cole et al., 2002; Gershunov and Barnett, 1998; Hamlet and Lettenmaier, 2007; Hunter et al., 2006; McCabe and Dettinger, 1999). When PDO is in its positive phase, El Niño events may be more extreme and exhibit wetter conditions; during a negative PDO, La Niña event are more frequent (Gershunov and Barnett, 1998; Gutzler et al., 2002; Lapp et al., 2013).

2.3 Study Area

Pajaro Valley is located on the Central Coast of California and comprises the coastal portion of the Pajaro River Watershed that borders the Monterey Bay Pajaro Valley

contains the city of Watsonville and other small towns such as Freedom and Las Lomas. Approximately 40% of the area serviced by the Pajaro Valley Water Management Agency (PVWMA) is agricultural land, 47% is natural vegetation, and 13% is urban land (Hanson et al., 2014). Pajaro Valley is one of the most productive agricultural regions in the world, with crop value estimated at over \$900 million annually (Hanson et al., 2014; PV Water, 2014). Pajaro Valley is completely reliant on groundwater to irrigate crops; nearly 100% of irrigated agriculture is supported by groundwater from the coastal aquifer system (PV Water, 2014). As a result, Pajaro has been experiencing seawater intrusion since the 1950s due to groundwater overdraft, a common issue for coastal aquifers. Surface water from diverted creeks, streams, and rivers is used for urban supply, while pumped groundwater is the primary supply of irrigated agriculture. Demand for water in the valley has increased due to population growth and the transition to water intensive crops. As a result, there has been an average groundwater overdraft of 12,950 acre-feet (15,973,566 m³) per year (Hanson et al., 2014). These current conditions create critical challenges in the WEF Nexus of Pajaro Valley, in addition to the climate-driven factors already affecting the hydrologic system (Hanson et al., 2014; Wada et al., 2016).

Surface water and groundwater in Pajaro Valley are used as input for agricultural production (Wada et al., 2016). The Pajaro Valley hydrologic system starts with inflows from precipitation and streamflow. Streamflow enters the valley in the Pajaro River through the Chittenden gap and as runoff from the local stream networks. Infiltration of runoff, along with infiltration of irrigation water, contributes to groundwater recharge (Hanson et

al., 2014). Like many coastal hydrological regions, Pajaro Valley is almost completely reliant on local groundwater for irrigation. Water issues in this area are aggravated by current and projected spatial problem of seawater intrusion. Future seawater intrusion will be determined by future groundwater pumping and climate variability (Wada et al., 2016). In addition to groundwater pumping, climate also affects the availability of groundwater for domestic and agricultural use. Climate change and climate variability have been identified as major stressors on the availability and sustainability of groundwater resources in California and other regions of the world (Green et al., 2011; Taylor et al., 2012).

3.0 METHODOLOGY

3.1 Data Selection

The observed and simulated data used in this study include climate indices, precipitation, streamflow discharge, groundwater levels, recharge volumes, and pumping volumes. All data sets are compiled on a monthly timescale; information for each dataset can be found in Table 1.

Observed data includes climate indices, precipitation, streamflow discharge, and groundwater levels. Climate indices were obtained from the Earth System Research Laboratory, Physical Sciences Division of NOAA (NOAA, 2019). I used the pre-1950 version of the MEI because several of the other data sets in this study start before 1950. MEI and PDO cover the period of 1908 through 2017. Precipitation data was obtained from California's Department of Water Resources (DWR) California Data Exchange Center or the Watsonville Water (WTW) meteorological station, and spans from 1908 through 2017.

This station is located in Watsonville, CA, and was selected due to its central location within the Pajaro Valley Watershed. The relatively long precipitation record length of 110 years (Table 1) also makes it a good choice for identifying ENSO and PDO signals.

Streamflow discharge data was obtained from a stream gauge (11159200) in the United States Geological Survey (USGS) National Water Information System (NWIS) (<https://waterdata.usgs.gov/nwis>). The stream gauge is located in Corralitos, CA and measures streamflow on the Corralitos Creek (COR). The data for the COR stream gauge spans from 1957 through 2017 and was selected due to its proximity to the WTW precipitation station and because it is the largest tributary in the valley. Groundwater level data was also obtained from USGS NWIS; one well (365231121482801012S001E24G001M) was selected due to the length and completeness of the record. This well is part of the California Coastal Basin aquifers system and has a depth of 61 m below land surface. The data spans from 1947 through 1983 and groundwater levels are measured in meters above or below land sea level.

Simulated data includes groundwater levels, recharge volumes, and pumping volumes with each data type containing an inland and coastal dataset. This data was generated as output of the Pajaro Valley Hydrologic Model (PVHM) developed using MODFLOW (Hanson et al., 2014). All data span from 1963 through 2014 with the exception of the groundwater level data that starts in 1964 (Table 1).

3.2 Time Series Analysis

Time series analysis was performed using the USGS Hydrologic and Climatic

Analysis Toolkit (HydroClimATe) (Dickinson et al., 2014). HydroClimATe is a computer program developed by the USGS for assessing the relations between variable climatic and hydrologic time-series data. The program automates methods such as time-series pre-processing, spectral analysis such as Fourier transform and Singular Spectrum Analysis (SSA), correlation analysis, and projections (Dickinson et al., 2014). For this study, I used HydroClimATe to pre-process data, perform SSA and lag correlations.

3.2.1 Data Pre-Processing

Several steps of preprocessing using HydroClimATe are necessary to remove any autocorrelation and anthropogenic signals from a time series and prepare the data for SSA. The preprocessing steps generally follow those outlined by Kuss and Gurdak (2014) and Hanson et al. (2006). These steps include interpolation, cumulative departure, detrending, and normalization using equations from Dickinson et al. (2014). Interpolation is used to estimate missing values within a data set. For this thesis, interpolation is used to give each data set a uniform monthly time interval by estimating values for months that are missing data. Once the data is interpolated, a cumulative departure curve is created, which is calculated as the sum of the differences between consecutive values in a timeseries and the mean of the series:

$$CD = \sum(x_i - \bar{x}) \quad (\text{Eq. 1})$$

where

CD is the cumulative departure curve
 x_i is the value at time i
 \bar{x} is the mean of the timeseries

The transformation of the time series to a cumulative departure allows intermittent temporal processes such as precipitation to be compared to persistent time series such as groundwater level data. The curve fitting method is then used to detrend each time series. A 3rd order polynomial is fit to a timeseries to represent the trend. Residuals for the timeseries are calculated as the difference between the fitted polynomial and the timeseries at time t . These residuals represent the time series with the trend removed (Dickinson et al., 2014). The residuals are then standardized to create normalized departures from the historic mean, which facilitates statistical comparisons among many different data types for correlation. Standardization transforms normally distributed variables to a new variable that has a sample mean equal to zero and a sample standard deviation equal to one:

$$z_i = \frac{x_i - \bar{x}}{s} \quad (\text{Eq. 2})$$

where

z_i is the normalized variable,
 x_i is the mean of the original timeseries,
 \bar{x} is the sample mean of the timeseries, and
 s is the sample standard deviation

These preprocessing steps were performed on each timeseries to prepare for SSA. The reader is directed to Dickinson et al. (2014) for additional details about the preprocessing and Singular Spectrum Analysis (SSA) methods.

3.2.2 Singular Spectrum Analysis (SSA)

SSA is a nonparametric method of principal component analysis that has been widely used to detect quasi-periodic oscillations and other interannual to multidecadal oceanic-atmospheric phenomena hydrologic time-series (Hanson et al., 2004; Kuss and Gurdak, 2014; Vautard et al., 1992). SSA was chosen for this analysis because it is useful in analyzing short, noisy timeseries, and assumes quasi-periodic rather than periodic oscillations. In this thesis, SSA is performed on the normalized departures of each individual climate index, precipitation, streamflow discharge, groundwater level, simulated recharge and pumping time-series. The purpose of SSA is to decompose the original time-series into independent and interpretable, reconstructed components (RCs) that can be interpreted as oscillatory patterns. No information is lost in the reconstruction process because the sum of these individual RCs equal the original time series (Ghil et al., 2002; Hanson et al., 2004; Hassani, 2007). My analysis follows the steps that are outlined in Dickinson et al. (2014). The SSA starts by utilizing a trajectory matrix X is composed of a series of windows of the time series that have a length of M . The dimensions of the trajectory matrix are M_T by N_T :

where

N_T is equal to $N-M+1$,
 N is the number of time steps in the timeseries, and
 M_T is the embedding dimension of X .

This is then used to construct the covariance matrix C :

$$C = \frac{DD^T}{N_T} \quad (\text{Eq. 3})$$

where

C is an M_T by M_T covariance matrix,
 D is an M_T by N_T trajectory matrix, and
 D^T is the transpose of X .

Then, the eigenvectors and eigen values of C are obtained by the eigenanalysis of C in the following form:

$$CE = \lambda E \quad (\text{Eq. 4})$$

where

E is an M_T by M_T matrix of the eigenvectors, and
 λ is the vector of eigenvalues of length M_T .

A matrix of the principal components A , is obtained by projecting the eigenvectors E onto the trajectory matrix D :

$$A = E^T D \quad (\text{Eq. 5})$$

where

E is an M_T by M_T matrix of the eigenvectors, and
 A is an M_T by N_T matrix of the principal components.

The RCs are then formed from the following:

$$RC = \frac{1}{M_t} \sum_{k \in K} \sum_{j=L_t}^{U_t} A_K(t-j+1) E_k(j) \quad (\text{Eq. 6})$$

where

- K is the set of eigenvectors that are used in the reconstruction,
- M_t is a normalization factor,
- L_t is a bound of summation, and
- U_t is a bound of summation.

The values of M_t, L_t, and U_t vary depending on the interval within the time series:

$$(M_t, L_t, U_t) = \left\{ \begin{array}{ll} \left(\frac{1}{t}, 1, t \right), & 1 \leq t \leq M_T - 1 \\ \left(\frac{1}{M_T}, 1, M_T \right), & M_T \leq t \leq N_T \\ \left(\frac{1}{N-t+1}, t - N + M_T, M_T \right), & N_T + 1 \leq t \leq N \end{array} \right\} \quad (\text{Eq. 7})$$

The majority of the variance within each hydrologic time-series is captured in the first 10 RCs, along with statistically significant oscillatory patterns for each data type. The Ghil and Mo significance test was used to determine which of these 10 RCs were statistically significant against a red-noise null hypothesis (Ghil and Mo, 1991). For each time-series, composite RCs were created from statistically significant RCs that fall within the periodicity ranges of ENSO and PDO. The composite RCs are calculated by grouping and summing the significant RCs by the following period ranges: 2-7 years (ENSO-composite), 12-35 (PDO-composite). By summing RCs based on similar period ranges, composite RCs are created that represent significant oscillatory modes within each time series that are consistent with ENSO or PDO (Gurdak et al., 2007; Kuss and Gurdak, 2014). These ENSO-composite and PDO-composite RCs are used for lag correlation analyses.

3.2.3 Lag Correlations

Measuring the delayed response of one hydrologic variable to another is useful for assessing their relationship in a hydrologic system. Lag correlations measure the strength of association between two variables at different time shifts by calculating lag correlation coefficients (Helsel and Hirsch, 2002). Lag correlations were performed following the methods from Kuss and Gurdak (2014) and Velasco et al. (2015). Before each correlation, the explanatory and response composite RCs were truncated to have the same start and end date, i.e. climate index truncated to match the length of the precipitation record, precipitation truncated to match groundwater levels, etc. HydroClimATe reports both forward and backward lags between two time-series; only the first 60 months (5 years) of forward lags were considered based on the previous work of Hanson et al. (2006, 2004). Hanson et al. (2006, 2004) studied aquifers in the southwestern U.S. and found that lag times of groundwater level correlations to ENSO and PDO fell within a range of 7 months to 5 years. Additionally, positive and negative correlation coefficients were reported based on known and assumed connections between the explanatory and response variables. For example, the positive (negative) phase of ENSO and PDO is known to increase (decrease) precipitation in central California, therefore I evaluated only the positive correlation coefficients between climate indices and precipitation. I evaluated only negative correlation coefficients between inverse relationships such as precipitation and observed groundwater because as precipitation increases (decreases) the depth to groundwater decreases (increases). Correlation coefficients were calculated for each monthly time lag

using a 95% confidence level; coefficients above this level were considered statistically significant.

4.0 RESULTS AND DISCUSSION

4.1 Percent Variance of Climate Variability Signals in Hydrologic Time Series

Results of the SSA showed that each time series contained statistically significant oscillatory signals that can be attributed to ENSO and PDO (Appendix A). The RCs consistent with ENSO were detected more frequently than PDO components. Of the hydrologic time series, ENSO was detected in 38.8% (31 of 80) of the RCs and PDO was detected in 20% (16 of 80) of the RCs (Appendix A). The amount of variance in the RCs attributed to ENSO for observed time-series ranged from 6 to 14% and from 1 to 5% for simulated time-series (Table 2). Although the variance in RCs associated with ENSO was detected more frequently, the PDO accounts for the largest amount of variance in RCs for both observed and simulated time-series (Table 2). For observed hydrologic data, PDO ranged from 30 to 85%, and from 77 to 98% variance (Table 2). These results are consistent with previous findings from Gurdak et al. (2007), Kuss (2011), Kuss and Gurdak (2014), and Velasco et al. (2015), that lower frequency climate oscillations tend to contain most of the variance in hydrologic time-series as compared to higher frequency oscillations.

4.2 Lag Correlations

Results in this section are organized by explanatory variable in the lag correlations; headings denote the explanatory variable (climate, precipitation, and groundwater). These explanatory variables are systematically correlated to all other inflows (precipitation,

streamflow, recharge) and outflows (pumping). Groundwater levels are considered responses to changes in inflows and outflows and discussed as a dependent variable. Results are organized by explanatory variable to inflows and to outflows, and inflows and outflows to groundwater levels.

4.2.1 Climate

Results of the lag correlations between climate indices and hydrologic inflows (precipitation, streamflow discharge, and simulated recharge) are shown in Table 3, Figure 3; results of the lag correlation between climate indices and hydrologic outflows (pumping) are shown in Table 4, Figure 4. Climate-precipitation lag correlations resulted in higher minimum, maximum, and average correlation coefficients for the ENSO correlations than the PDO (Table 3, Figure 3). Although they were higher ENSO, the correlation coefficients showed a low to moderate maximum correlation (0.31) between ENSO and observed precipitation with an average lag time of approximately 1 year (Table 3, Figure 3). The lag correlations were low (0.12) between PDO and observed precipitation with an average lag time of approximately 2 years.

The results of the lag correlations between climate and streamflow (Table 3, Figure 3) have the opposite relative correlation strength between ENSO and PDO as compared to the climate-precipitation lag correlations (Table 3, Figure 3). PDO had the highest maximum correlation to streamflow with a maximum correlation coefficient of 0.60 and a lag of 1 year, which was the highest lag correlation coefficient between climate and any

inflow. Streamflow had the shortest average lag (0.63 years) to ENSO variability and average lag of 2 years to PDO.

Simulated recharge (Table 3, Figure 3) was moderately correlated to climate for both coastal and inland locations with average correlation coefficients ranging from 0.20 to 0.35. ENSO had the stronger correlation to simulated recharge (0.42 coastal, 0.47 inland) compared to PDO (0.25 coastal, 0.37 inland) (Table 3, Figure 3). The average lag times range from 0.71 to 0.75 years for ENSO and 1.3 and 1.6 for PDO (Table 3, Figure 3). For correlations between climate and hydrologic inflows (precipitation, streamflow, recharge), ENSO had higher correlation coefficient values with simulated data than observed while correlation coefficients for observed data were higher for PDO than simulated.

Correlations between climate and hydrologic outflows (pumping) resulted in similar maximum correlation coefficients for ENSO (-0.24) and PDO (-0.26) (Table 4, Figure 4). These maximum correlations represent a near immediate response because the lags range from 0 to 0.25 months (Table 4, Figure 4). The average lag time between climate and groundwater pumping ranges between 0.5 to 2.5 years, with ENSO RCs having the shortest average lag at 0.5 years.

4.2.2 Precipitation

Results for the lag correlations between precipitation and hydrologic inflows (streamflow discharge and recharge) can be found in Table 5, Figure 5; results for lag correlations between precipitation and hydrologic outflows (pumping) can be found in Table 6, Figure 6. Precipitation and streamflow were strongly correlated with coefficients

of 0.80 (ENSO-composite) and 0.87 (PDO-composite) (Table 5, Figure 5). Groundwater recharge was strongly correlated to precipitation and had maximum correlation coefficients that ranged between 0.71 to 0.80 (Table 6, Figure 6). ENSO-composite RCs for streamflow and groundwater recharge had an immediate response to ENSO-composite precipitation RCs with a lag time of 0 years for both maximum correlations. PDO-related recharge RCs reached maximum correlation of 0.71 (coastal recharge) and 0.80 (inland recharge) at a 0.2-year lag (Table 5, Figure 5b). Lag correlations for precipitation to hydrologic inflows (streamflow, recharge) had similar correlation coefficients for both ENSO and PDO-composite RCs, and slightly higher correlation coefficients for observed data (streamflow) than simulated data (recharge).

Lag correlations between precipitation and groundwater pumping (hydrologic outflows) RCs resulted in weaker correlations to ENSO-composite RCs than the PDO-composite RCs (Table 6, Figure 6). Average correlation coefficients between precipitation and pumping ranged from -0.13 to -0.31 with an average lag of 0.5 years to ENSO-composite precipitation and 2.5 years for PDO-composite precipitation.

4.2.3 Groundwater

Results for correlation of climate indices to groundwater levels are shown in Table 7, Figure 7; hydrologic inflows (precipitation, streamflow discharge, and recharge) to groundwater level results are shown in Table 8, Figures 8 and 9; hydrologic outflows (pumping) to groundwater level results are shown in Table 9, Figure 10. Correlations between climate index RCs and groundwater level RCs, for both observed and simulated

groundwater levels, had similar maximum correlation coefficients for ENSO and PDO that ranged between 0.44 and 0.48 (Table 7, Figure 7 and 8). Observed groundwater levels had the stronger correlation to ENSO climate index (MEI) (0.44) and the longest average lag time of approximately 3.3 years (Table 7, Figure 7a), as compared to the simulated groundwater levels (Table 7, Figure 8a). Simulated groundwater levels had similar correlation coefficients to ENSO and PDO (Table 7, Figure 8) with values ranging from 0.42 to 0.48, and corresponding lag time ranging from 0.75 to 2.5 years. Simulated groundwater levels had the shortest average lag time to ENSO of 1.5 (coastal) and 1.7 (inland) years.

For precipitation to groundwater levels, observed data had a moderate maximum correlation coefficient of 0.43 to ENSO-composite composite RCs, and a strong maximum correlation of 0.65 to PDO-composite RCs (Table 8, Figure 8). Simulated groundwater levels had the opposite relationship, with stronger maximum correlations between ENSO-composite RCs (0.67-0.72) than PDO-composite RCs (0.5-0.59) (Table 8, Figure 9). PDO-composite RCs also had a consistent average lag time of 2.5 years for both observed and simulated groundwater level data (Table 8, Figure 8b and 9b). ENSO-composite RCs had average lag times that ranged from 0.92 to 3 years.

Lag correlations between streamflow discharge to groundwater levels resulted in a strong relationship between the two variables. Observed and simulated (Table 8, Figure 8 and 9) groundwater levels had similar correlation coefficients that ranged between 0.62 to 0.77 indicating a strong correlation between streamflow and groundwater levels between

both ENSO-composite and PDO-composite composite RCs. The exception was between ENSO-related streamflow and observed groundwater levels which had a correlation of 0.28. Groundwater levels had an average lag of 0.5 to 2.5 years to streamflow.

Groundwater levels were moderately to strongly correlated to simulated recharge with maximum correlation coefficients ranging from 0.51 to 0.87 for observed groundwater levels (Table 8, Figure 8) and 0.63 to 0.68 for simulated groundwater levels (Table 8, Figure 9). Both ENSO-related correlations had an average lag of 0.75-0.92 years. Observed groundwater (Table 8, Figure 8) levels had a stronger correlation among PDO-composite recharge RCs (0.82-0.87) than ENSO-composite composite RCs (0.51-0.52) while simulated groundwater levels (Table 8, Figure 9) had similar correlations to both ENSO and PDO-composite recharge RCs.

Correlations between groundwater pumping and groundwater levels resulted in a moderate to strong relationship (Table 9, Figure 10). Observed groundwater levels (Table 17) had a moderate maximum correlation to simulated pumping (-0.41, coastal and inland), which was an immediate response at a lag of 0 years for ENSO-composite composite RCs. Correlations among the PDO-composite composite RCs resulted in maximum correlation coefficients of -0.36 for coastal groundwater pumping and -0.37 for inland (Table 9, Figure 10b). Although the correlations were about the same, the lag time ranged between 0.75 years (inland) and 5 years (coastal). The average lag for these PDO-composite RCs also ranged from 1 (inland) to 4.7 (coastal) years. Simulated groundwater levels also resulted in a range of values and lag times to simulated pumping (Table 9, Figure 10b). ENSO-

composite composite RC correlations resulted in a moderate relationship (-0.37, inland; -0.57, coastal) to simulated pumping with lag times ranging from 0.5 years (coastal) to 1.3 years (inland). Simulated groundwater levels had a strong correlation to simulated pumping among the PDO-composite RCs. Coastal pumping to groundwater levels had the strongest correlation of -0.9 with a lag of 0 months; inland pumping had a correlation of -0.73 with a lag of 2 years (Table 9, Figure 10).

4.3 How does climate affect the water for food relationship within the WEF Nexus of Pajaro Valley?

To address this first of three research questions, I found that climate variability has a moderate to strong relationship to water availability in the Pajaro Valley Watershed. The highest correlation coefficients were between ENSO and precipitation and simulated groundwater recharge. Inland simulated recharge also had a slightly stronger response to ENSO than coastal recharge. Although I anticipated the surface hydrology in Pajaro Valley would respond to ENSO, I expected precipitation to have the strongest response to both ENSO and PDO compared to streamflow and recharge. However, the strongest correlation of all inflows was between PDO and streamflow discharge; the weakest correlation was between PDO and precipitation.

Based on the percent variance of ENSO and PDO in the precipitation time-series (Table 2), it would be expected that PDO would have a stronger influence on temporal variability in precipitation; ENSO accounts for 6% of the variance and PDO accounts for 30%. RC 1 (Appendix A) in the time-series makes up 60% of the variance but was not

attributed to either ENSO or PDO due to its periodicity of 55 years. This signal could be attributed to 50-70 year low-frequency mode of PDO, which was not used in this analysis. Another possible reason for weak to average correlation coefficients between climate and precipitation could be the unpredictability of ENSO and PDO bringing high amounts of precipitation to the Central Coast of California. The visual representation of the ENSO and precipitation RCs (Figure 11) shows the unpredictability and differing trends between ENSO and precipitation. Precipitation is not always responding to the changes in the MEI index; in some places it appears to be preceding the index or exhibiting an inverse pattern.

The average lag time between climate and hydrologic inflows ranged from months to a maximum of 2 years. This time falls within the expected lag time of 7 months to 5 years outlined by Hanson et al., 2006. Responses to PDO were longer on average compared to responses to ENSO. This was expected due to the length of the period of fluctuation; PDO fluctuates less frequently than ENSO. If a period of fluctuation is longer (shorter), it will take more (less) time to reach the point of maximum correlation between two time-series. For ENSO-composite composite RCs, the correlation between climate and precipitation had the longest lag of 1.1 years. PDO had the longest lag (2 years) to streamflow discharge, but also a lag of 1.9 years to precipitation.

Despite having a weak to moderate correlation to climate, precipitation was strongly correlated to streamflow discharge and simulated groundwater recharge. This was expected due to the direct physical connection between precipitation and the surface hydrology. For the maximum correlations, the corresponding lag times ranged from 0 to 7

months. The lack of a lag between precipitation and streamflow can be attributed to the direct surface connection between the two. Having a lag that is on a scale of less than a month is another possibility. The timeseries of precipitation and streamflow (Figure 12) are in-phase and nearly identical, with a short time lag. The same near-instantaneous response also occurs between the precipitation-recharge timeseries (Figure 13) but is most likely related to the simplicity of the Pajaro Valley Hydrologic Model (MODFLOW) model in simulating water flux and travel time through the vadose zone that represents recharge.

Based on the timeseries of precipitation RCs and El Niño and La Niña events (Figure 14), there is a visual indication that precipitation patterns respond to ENSO which supports the results of the SSA and lag correlation analysis. However, as stated before, ENSO is a complex system of ocean and atmospheric interactions, and local precipitation patterns are not be completely driven by ENSO. There are places in the timeseries where a strong El Niño (La Niña) does not lead to the expected response of an increase (decrease) in precipitation. This pattern is also seen in the streamflow discharge timeseries (Figure 15). Streamflow responds to climate by discharge increasing (decreasing) during El Niño (La Niña) events. This is verified by the lag correlation results between climate indices and streamflow discharge. However, there are places in the timeseries where streamflow discharge is changing without the influence of ENSO such as the increase in discharge following the 1977 and preceding the 2007 La Niña events. Simulated recharge responds similarly (Figure 16) but both timeseries still generally respond to the changing phases of

ENSO. Local precipitation patterns not associated with climate variability will still cause a response in the surface hydrology.

4.4 How does climate influence human interactions in the hydrologic system in terms of groundwater pumping?

Despite 97% of the variance in the groundwater pumping record being attributed to ENSO and PDO (Table 2), pumping and climate are weakly correlated (Table 17). There is an inverse relationship between pumping and climate; pumping tends to increase (decrease) during dry (wet) periods due to the availability of water for use. The time-series comparing the MEI to simulated pumping (Figure 18) shows this general inverse pattern from 1977-2001, but after 2001 starts to show a trend of pumping increasing when ENSO is in its positive (wet) phase. This pattern change could be explained by the change in pumping practices in Pajaro and intensified agricultural practices following 1993 (Hanson et al., 2014).

Groundwater pumping is an anthropogenic forcing on the hydrologic system. Farmers choose when and how much to pump based on a variety of factors, such as precipitation, the availability of surface water, cropping patterns, irrigation methods, and market prices, among other factors. Since precipitation was only moderately correlated to modes of climate variability, it follows that groundwater pumping would have a low to moderate correlation as well. Crop value also influences how much groundwater is pumped, this occurred when farmers switched to higher value, water-intensive crops within Pajaro Valley (Hanson et al., 2014; PV Water, 2014).

Despite the moderate correlation to climate, groundwater pumping had a strong response to the surface water availability. Groundwater pumping RCs resulted in higher correlation coefficients to PDO-related RCs of precipitation and streamflow discharge. Lag correlation results for streamflow to groundwater pumping are reported in Appendix B. Similar to the results of climate to inflows, the higher correlation between PDO-composite RCs is due to the long period of fluctuation. PDO changes phase less frequently than ENSO and is able to capture long term changes within each timeseries. This long period of fluctuation resulted in relatively long lags of 4-5 years (Table 8). ENSO changes phase more frequently than PDO, and responses to these changes may be minimal or not present in the timeseries at all. Despite correlations between ENSO-composite RCs being low, they can also be used to represent an “immediate” human response due to short lags of 0-1 year.

Although I expected groundwater pumping to be strongly correlated to climate variability and precipitation, there are many factors involved in the process. I expected pumping to increase during dry periods (La Niña) and decrease during wet periods (El Niño). However, the process becomes complex due to the human interaction and motives to pump. Pajaro’s growing season is during the summer, when there is less precipitation. The decision and amount of pumping depends on the availability of surface water, which depends on how much rain occurred in the previous winter. The response rate of farmers to wet and dry periods is another factor. The timeseries of groundwater pumping (Figure 18) shows this responsiveness, which varies over several phases of ENSO. There are several places where there is increased (decreased) pumping during a wet (dry) period, this

contradiction could be a result of the lag time between the climate forcing and action by farmers. Also, farmers are more inclined to grow higher value crops that require more water. This demand for more water is independent of climate forcings and more dependent on market forcings and profit. There are large departures from the mean pumping volume after the 1993 switch to more intense agricultural practices. Despite the complexity surrounding pumping practices, groundwater pumping did respond to changing surface hydrology and the availability of surface water for use; we also see a lagged response to wet and dry periods.

4.5 To what extent does seawater intrusion respond to wet and dry periods?

Coastal aquifers are vulnerable to seawater intrusion due to the proximity to the ocean. Groundwater pumping increases this vulnerability by lowering the water table. Groundwater withdrawals over a long period of time will eventually create a cone of depression that will draw seawater into the aquifer (DWR, 2017; Werner et al., 2013). An example of this is when groundwater levels drop below sea level and seawater flows inland. To analyze whether seawater intrusion responds to wet and dry periods, I assume seawater intrusion occurs when the observed and simulated groundwater levels drop below sea level, 2.7 m below land surface.

In the 1940s, groundwater levels in Pajaro Valley were near surface level around the coast year round; seawater intrusion was first identified along the Monterey Bay in 1953 (PV Water, 2014). The raw observed groundwater levels (Figure 19a) mark the beginning of seawater intrusion in the Pajaro Valley. Between 1947 and 1975 seawater

intrusion occurred seasonally; groundwater head was below sea level during the summer growing season and rose above sea level in the winter by about the same amount prior to the growing season. This seasonality occurred after 1975 but groundwater head stayed below sea level for most of the year until the end of the record. The ENSO-composite RC timeseries (Figure 19b) shows that groundwater levels and seawater intrusion respond to wet (El Niño) and dry (La Niña) periods. Groundwater levels respond to wet, strong El Niño events for the 1957-1960, 1965-1967, and 1982-1983 periods; during these periods groundwater levels were above sea level. However, these responses are followed by sharp declines in groundwater levels at the middle or end of these events. The 1972-1974 El Niño event occurred after two La Niña events, resulting in groundwater levels rising above sea level after a three-year decline. Similar to the other strong El Niño periods, this rise in groundwater head was followed by a sharp decline. There are similar declines following the moderate El Niño events but on a smaller scale following small increases in groundwater head. During dry La Niña periods, groundwater levels are below sea level for the 1949-1951, 1954-1956, and 1974-1975 periods. These periods of seawater intrusion are followed by increases in groundwater head, similar to the declines in groundwater head following El Niño periods.

The simulated record of groundwater levels begins a decade after the identification of seawater intrusion in the valley and shows the gradual advancement of seawater intrusion from the coastal to the inland area. Groundwater levels in the coastal area (Figure 20a) are below sea level for the entirety of the record. However, groundwater levels rose

above sea level during and following winters in which there was an El Niño event such as 1967-1971, 1973-1975, 1983-1984, and 2004-2006. The inland area (Figure 20b) did not experience seawater intrusion until 1989, following seasonal declines throughout the mid-1980s and the strong La Niña during 1988-1991. Groundwater levels did rise above sea level following the 1997-1999 El Niño throughout the growing season but declined again following the 2007-2009 La Niña. The ENSO-composite timeseries (Figure 20c) shows the coastal and inland areas responding similarly to wet and dry periods. Prior to changing agricultural practices in 1993, groundwater levels in the coastal and inland area responded to wet and dry periods consistently and similarly. The behavior of the coastal and inland timeseries deviate from each other following 1993 and lose the consistent response to El Niño and La Niña events.

For both observed and simulated records of groundwater levels, there is a response of seawater intrusion to wet (El Niño) and dry (La Niña) periods. However, seawater intrusion is also greatly affected by the physical surface processes such as precipitation, groundwater recharge, and groundwater pumping. Results of the lag correlations between groundwater levels and climate, precipitation, recharge, and groundwater pumping verify the connection of seawater intrusion to climate and physical processes. The response of seawater intrusion to changes in the MEI Index and precipitation is lagged by 0.67-3 years based on correlating changes in groundwater head to known periods of strong to moderate El Niño and La Niña events (Figure 19, 20). The lag correlations between climate and observed and simulated groundwater levels (Table 7), verify this delayed response. This

same delayed response is also verified in the correlations between precipitation and observed and simulated (Table 8) groundwater levels. However, changes in groundwater recharge and pumping also affect the occurrence of seawater intrusion but on a shorter timescale. Changes in groundwater recharge are directly and physically connected to groundwater levels. As a result, groundwater levels respond quickly to groundwater recharge (0.5-1 year; Table 8). Changes in groundwater pumping, the cause of seawater intrusion, also influences groundwater levels quickly (0-1 year; Table 9).

Changes in groundwater recharge as a result of climate variability affect groundwater levels and the magnitude of seawater intrusion. Groundwater pumping, which is not always driven by climatic factors, also directly affect seawater intrusion. While seawater intrusion does respond to wet and dry periods, it is also responding conjunctively to surface hydrological processes and human interaction, both of which may or may not be occurring as a result of modes of climate variability.

5.0 CONCLUSION

Modes of climate variability such as the ENSO and PDO were shown to have a moderate to strong influence on hydrologic processes in the Pajaro Valley. The use of SSA and lag correlations verified this influence by identifying signals in each timeseries that can be attributed to ENSO and PDO and the response of hydrologic variables to these signals. Although the PDO accounted for the highest amount of variance in each timeseries, several parts of the hydrologic system were highly correlated to both ENSO and PDO. The surface hydrology (streamflow discharge and simulated recharge) was strongly influenced

by variations of precipitation which responded irregularly to phases of ENSO and PDO. However, surface-water responded strongly to precipitation, showing surface-water availability is dependent on climatic factors.

Anthropogenic forcings on the hydrologic system in the form of groundwater pumping responded moderately and irregularly to changes in surface water availability and climate. Farmers are motivated to pump groundwater for a variety of reasons, which adds to the complexity of the water-food relationship within the WEF Nexus. Seawater intrusion does respond to wet and dry periods but also responds to changes in surface processes such as high amounts of precipitation increasing surface-water availability. Human interactions also drive seawater intrusion as groundwater pumping is directly related to declines in groundwater levels. Surface-water serves a crucial mediator within the WEF Nexus of Pajaro Valley. It is strongly correlated to climate variability and heavily influences groundwater levels and pumping practices. When surface water is abundant it alleviates the dependence on groundwater for agriculture. With proper management and the implementation of sustainable agricultural practices, surface-water can aid in reducing seawater intrusion and reduce conflict within the water for food linkage within the WEF Nexus.

REFERENCES

- Anderson, W.P., Emanuel, R.E., 2008. Effect of interannual and interdecadal climate oscillations on groundwater in North Carolina. *Geophysical Research Letters* 35, 4. <https://doi.org/10.1029/2008GL036054>
- Brabets, T.P., Walvoord, M.A., 2009. Trends in streamflow in the Yukon River Basin from 1944 to 2005 and the influence of the Pacific Decadal Oscillation. *Journal of Hydrology* 371, 108–119. <https://doi.org/10.1016/j.jhydrol.2009.03.018>
- Brown, D.P., Comrie, A., 2004. A winter precipitation “dipole” in the western United States associated with multidecadal ENSO variability. *Geophysical Research Letters* 31.
- Cayan, D.R., Redmond, K.T., Riddle, L.G., 1999. ENSO and Hydrologic Extremes in the Western United States*. *Journal of Climate* 12, 2881–2893.
- CDFA, 2016. California Agricultural Exports 2015-2016 (Government Report). Sacramento, CA.
- Chikamoto, Y., Timmermann, A., Luo, J.-J., Mochizuki, T., Kimoto, M., Watanabe, M., Ishii, M., Xie, S.-P., Jin, F.-F., 2015. Skillful multi-year predictions of tropical trans-basin climate variability. *Nature Communications* 6, 7. <https://doi.org/10.1038/ncomms7869>
- Cole, J.E., Overpeck, J.T., Cook, E.R., 2002. Multiyear La Niña events and persistent drought in the contiguous United States. *Geophysical Research Letters* 29, 4. <https://doi.org/10.1029/2001GL013561>
- Dickinson, J.E., Hanson, R.T., Ferré, T.P.A., Leake, S.A., 2004. Inferring time-varying recharge from inverse analysis of long-term water levels. *Water Resources Research* 40, 15. <https://doi.org/10.1029/2003WR002650>
- Dickinson, J.E., Hanson, R.T., Predmore, S.K., 2014. HydroClimATe—Hydrologic and Climatic Analysis Toolkit, in: *Hydrologic Analysis and Interpretation, Techniques and Methods*. U.S. Geological Survey, Reston, Virginia, p. 48.
- DWR, 2017. Best Management Practices for the Sustainable Management of Groundwater.
- Earman, S., Dettinger, M., 2011. Potential impacts of climate change on groundwater resources – a global review. *Journal of Water and Climate Change* 2, 213. <https://doi.org/10.2166/wcc.2011.034>
- Endo, A., Burnett, K., Orenco, P., Kumazawa, T., Wada, C., Ishii, A., Tsurita, I., Taniguchi, M., 2015. Methods of the Water-Energy-Food Nexus. *Water* 7, 5806–5830. <https://doi.org/10.3390/w7105806>
- Famiglietti, J.S., 2014. The global groundwater crisis. *Nature Climate Change* 4, 945–948. <https://doi.org/10.1038/nclimate2425>
- Ferguson, G., Gleeson, T., 2012. Vulnerability of coastal aquifers to groundwater use and climate change. *Nature Climate Change* 2, 342–345.

- Fleming, S.W., Quilty, E.J., 2006. Aquifer Responses to El Niño-Southern Oscillation, Southwest British Columbia. *Ground Water* 44, 595–599.
<https://doi.org/10.1111/j.1745-6584.2006.00187.x>
- Food and Agriculture Organization of the United Nations, 2014. *The Water-Energy-Food Nexus: a new approach in support of food security and sustainable agriculture*. Food and Agriculture Organization for the United Nations, Rome.
- Gershunov, A., Barnett, T.P., 1998. Interdecadal Modulation of ENSO Teleconnections. *Bulletin of the American Meteorological Society* 79, 2715–2725.
- Ghil, M., 2002. Natural Climate Variability, in: *Encyclopedia of Global Environmental Change, The Earth System: Physical and Chemical Dimensions of Global Environmental Change*. Wiley, Chichester ; New York, p. 6.
- Ghil, M., Allen, M.R., Dettinger, M.D., Ide, K., Kondrashov, D., Mann, M.E., Robertson, A.W., Saunders, A., Tian, Y., Varadi, F., Yiou, P., 2002. Advanced Spectra Methods for Climatic Time Series. *Reviews of Geophysics* 40, 41.
<https://doi.org/10.1029/2000RG000092>
- Ghil, M., Mo, K.T., 1991. Intraseasonal Oscillations in the Global Atmosphere. *Journal of the Atmospheric Sciences* 48, 752–790.
- Gurdak, J.J., 2017. Groundwater: Climate-induced pumping. *Nature Geoscience* 10.
<https://doi.org/doi:10.1038/ngeo2885>
- Gurdak, J.J., Hanson, R.T., Green, T.R., 2009. *Effects of Climate Variability and Change on Groundwater Resources of the United States (Fact Sheet No. 2009–3074)*. U.S. Geological Survey, Lakewood, Colorado.
- Gurdak, J.J., Hanson, R.T., McMahan, P.B., Bruce, B.W., McCray, J.E., Thyne, G.D., Reedy, R.C., 2007. Climate variability controls on unsaturated water and chemical movement, High Plains aquifer, USA. *Vadose Zone Journal* 6, 533.
<https://doi.org/10.2136/vzj2006.0087>
- Gutzler, D.S., Kann, D.M., Thornbrugh, C., 2002. Modulation of ENSO-Based Long-Lead Outlooks of Southwestern U.S. Winter Precipitation by the Pacific Decadal Oscillation. *Weather and Forecasting* 17, 1163–1172.
- Hamlet, A.F., Lettenmaier, D.P., 2007. Effects of 20th century warming and climate variability on flood risk in the western U.S. *Water Resources Research* 43, 17.
<https://doi.org/10.1029/2006WR005099>
- Hanson, R.T., Dettinger, M.D., Newhouse, M.W., 2006. Relations between climatic variability and hydrologic time series from four alluvial basins across the southwestern United States. *Hydrogeology Journal* 14, 1122–1146.
<https://doi.org/10.1007/s10040-006-0067-7>
- Hanson, R.T., Newhouse, M.W., Dettinger, M.D., 2004. A methodology to assess relations between climatic variability and variations in hydrologic time series in the southwestern United States. *Journal of Hydrology* 287, 252–269.
<https://doi.org/10.1016/j.jhydrol.2003.10.006>
- Hanson, R.T., Schmid, W., Faunt, C.C., Lear, J., Lockwood, B., 2014. *Integrated Hydrologic Model of Pajaro Valley, Santa Cruz and Monterey Counties*,

- California (Scientific Investigations Report No. 5111). U.S. Department of the Interior, U.S. Geological Survey.
- Hassani, H., 2007. Singular Spectrum Analysis: Methodology and Comparison. *Journal of Data Science* 5, 239–257.
- Helsel, D.R., Hirsch, R.M., 2002. Chapter A3: Statistical Methods in Water Resources, in: *Techniques of Water Resources Investigations, Book 4*. U.S. Geological Survey, p. 522.
- Higgins, R.W., Silva, V.B.S., Shi, W., Larson, J., 2007. Relationships between Climate Variability and Fluctuations in Daily Precipitation over the United States. *Journal of Climate* 20, 3561–3579. <https://doi.org/10.1175/JCLI4196.1>
- Hoff, H., 2011. Understanding the Nexus, in: *Background Paper for the Bonn2011 Conference*. Presented at the The Water, Energy and Food Security Nexus, Stockholm Environmental Institute, Stockholm.
- Holman, I.P., 2006. Climate change impacts on groundwater recharge - uncertainty, shortcomings, and the way forward? *Hydrogeology Journal* 14, 637–647. <https://doi.org/10.1007/s10040-005-0467-0>
- Holman, I.P., Rivas-Casado, M., Bloomfield, J.P., Gurdak, J.J., 2011. Identifying non-stationary groundwater level response to North Atlantic ocean-atmosphere teleconnection patterns using wavelet coherence. *Hydrogeology Journal* 19, 1269–1278. <https://doi.org/10.1007/s10040-011-0755-9>
- Hunter, T., Tootle, G., Piechota, T., 2006. Oceanic-atmospheric variability and western U.S. snowfall. *Geophysical Research Letters* 33, 5. <https://doi.org/10.1029/2006GL026600>
- Hurrell, J.W., Kushnir, Y., Ottersen, G., Visbeck, M., 2003. An overview of the North Atlantic Oscillation, in: Hurrell, J.W., Kushnir, Y., Ottersen, G., Visbeck, M. (Eds.), *Geophysical Monograph Series*. American Geophysical Union, Washington, D. C., pp. 1–35.
- Kiladis, G.N., Diaz, H.F., 1989. Global Climatic Anomalies Associated with Extremes in the Southern Oscillation. *Journal of Climate* 2, 1069–1090.
- Kondrashov, D., Feliks, Y., Ghil, M., 2005. Oscillatory modes of extended Nile River records (A.D. 622–1922). *Geophysical Research Letters* 32, 4. <https://doi.org/10.1029/2004GL022156>
- Konikow, L.F., Kendy, E., 2005. Groundwater depletion: A global problem. *Hydrogeology Journal* 13, 317–320. <https://doi.org/10.1007/s10040-004-0411-8>
- Kuss, A.J.M., 2011. Effects of climate variability on recharge in regional aquifers of the United States. San Francisco State University, San Francisco, CA.
- Kuss, A.J.M., Gurdak, J.J., 2014. Groundwater level response in U.S. principal aquifers to ENSO, NAO, PDO, and AMO. *Journal of Hydrology* 519, 1939–1952. <https://doi.org/10.1016/j.jhydrol.2014.09.069>
- Lapp, S.L., St. Jacques, J.-M., Sauchyn, D.J., Vanstone, J.R., 2013. Forcing of hydroclimatic variability in the northwestern Great Plains since AD 1406. *Quaternary International* 310, 47–61. <https://doi.org/10.1016/j.quaint.2012.09.011>

- Leck, H., Conway, D., Bradshaw, M., Rees, J., 2015. Tracing the Water-Energy-Food Nexus: Description, Theory and Practice: Tracing the Water-Energy-Food Nexus. *Geography Compass* 9, 445–460. <https://doi.org/10.1111/gec3.12222>
- Liu, Q., 2017. WEF Nexus Cases from California with Climate Change Implication. *Water-Energy-Food Nexus: Principles and Practices* 229, 151.
- Mantua, N.J., Hare, S.R., 2002. The Pacific decadal oscillation. *Journal of Oceanography* 58, 35–44.
- Masterson, J.P., Garabedian, S.P., 2007. Effects of Sea-Level Rise on Ground Water Flow in a Coastal Aquifer System. *Ground Water* 45, 209–217. <https://doi.org/10.1111/j.1745-6584.2006.00279.x>
- Mazouz, R., Assani, A.A., Quessy, J., Légaré, G., 2012. Comparison of the interannual variability of spring heavy flood characteristics of tributaries of the St. Lawrence River in Quebec (Canada). *Advances in Water Resources* 35, 110–120. <https://doi.org/10.1016/j.advwatres.2011.10.006>
- McCabe, G.J., Dettinger, M.D., 1999. Decadal variations in the strength of ENSO teleconnections with precipitation in the western United States. *International Journal of Climatology* 19, 1399–1410.
- McCabe, G.J., Palecki, M.A., Betancourt, J.L., 2004. Pacific and Atlantic Ocean influences on multidecadal drought frequency in the United States. *Proceedings of the National Academy of Sciences* 101, 4136–4141. <https://doi.org/10.1073/pnas.0306738101>
- NOAA, 2018. National Climatic Data Center.
- NOAA, ESRL, 2019. Physical Sciences Division.
- Perez-Valdivia, C., Sauchyn, D., Vanstone, J., 2012. Groundwater levels and teleconnection patterns in the Canadian Prairies. *Water Resources Research* 48, 13. <https://doi.org/10.1029/2011WR010930>
- Pool, D.R., 2005. Variations in climate and ephemeral channel recharge in southeastern Arizona, United States. *Water Resources Research* 41, 25. <https://doi.org/10.1029/2004WR003255>
- PV Water, 2014. Basin Management Plan Update (Final). Pajaro Valley Water Management Agency.
- Ropelewski, C.F., Halpert, M.S., 1987. Global and regional scale precipitation patterns associated with the El Niño/Southern Oscillation. *Monthly Weather Review* 115, 1606–1626.
- Ropelewski, C.F., Halpert, M.S., 1986. North American Precipitation and Temperature Patterns Associated with the El Niño/Southern Oscillation (ENSO). *Monthly Weather Review* 114, 2352–2362.
- Sabziparvar, A.A., Mirmasoudi, S.H., Tabari, H., Nazemosadat, M.J., Maryanaji, Z., 2011. ENSO teleconnection impacts on reference evapotranspiration variability in some warm climates of Iran. *Journal of Climatology* 31, 1710–1723. <https://doi.org/10.1002/joc.2187>

- Schonher, T., Nicholson, S.E., 1989. The Relationship between California Rainfall and ENSO Events. *Journal of Climate* 2, 1258–1269.
- Shang, H., Yan, J., Zhang, X., 2011. El Niño–Southern Oscillation influence on winter maximum daily precipitation in California in a spatial model. *Water Resources Research* 47. <https://doi.org/10.1029/2011WR010415>
- Smidt, S.J., Haacker, E.M.K., Kendall, A.D., Deines, J.M., Pei, L., Cotterman, K.A., Li, H., Liu, X., Basso, B., Hyndman, D.W., 2016. Complex water management in modern agriculture: Trends in the water-energy-food nexus over the High Plains Aquifer. *Science of The Total Environment* 566–567, 988–1001. <https://doi.org/10.1016/j.scitotenv.2016.05.127>
- Tremblay, L., Larocque, M., Anctil, F., Rivard, C., 2011. Teleconnections and interannual variability in Canadian groundwater levels. *Journal of Hydrology* 410, 178–188. <https://doi.org/10.1016/j.jhydrol.2011.09.013>
- Vautard, R., Pascal, Y., Ghil, M., 1992. Singular Spectrum Analysis: A toolkit for short, noisy, chaotic time series. *Physica D: Nonlinear Phenomena* 58, 95–126.
- Velasco, E.M., Gurdak, J.J., Dickinson, J.E., Ferré, T.P.A., Corona, C.R., 2015. Interannual to multidecadal climate forcings on groundwater resources of the U.S. West Coast. *Journal of Hydrology: Regional Studies*. <https://doi.org/10.1016/j.ejrh.2015.11.018>
- Venencio, M. del V., García, N.O., 2011. Interannual variability and predictability of water table levels at Santa Fe Province (Argentina) within the climatic change context. *Journal of Hydrology* 409, 62–70. <https://doi.org/10.1016/j.jhydrol.2011.07.039>
- Wada, C.A., Burnett, K., Gurdak, J.J., 2016. Sustainable Agriculture Irrigation Management: The Water-Energy-Food Nexus in Pajaro Valley, California. *Sustainable Agriculture Research* 5, 76. <https://doi.org/10.5539/sar.v5n3p76>
- Wada, Y., van Beek, L.P.H., van Kempen, C.M., Reckman, J.W.T.M., Vasak, S., Bierkens, M.F.P., 2010. Global depletion of groundwater resources. *Geophysical Research Letters* 37. <https://doi.org/10.1029/2010GL044571>
- Werner, A.D., Bakker, M., Post, V.E.A., Vandenbohede, A., Lu, C., Ataie-Ashtiani, B., Simmons, C.T., Barry, D.A., 2013. Seawater intrusion processes, investigation and management: Recent advances and future challenges. *Advances in Water Resources* 51, 3–26. <https://doi.org/10.1016/j.advwatres.2012.03.004>
- Whittemore, D.O., Butler, J.J., Wilson, B.B., 2016. Assessing the major drivers of water-level declines: new insights into the future of heavily stressed aquifers. *Hydrological Sciences Journal* 61, 134–145.
- Wolter, K., Timlin, M.S., 2011. El Niño/Southern Oscillation behaviour since 1871 as diagnosed in an extended multivariate ENSO index. *International Journal of Climatology* 31, 1074–1087. <https://doi.org/10.1002/joc.2336>
- Zhang, Y., Wallace, J.M., Battisti, D.S., 1997. ENSO-composite interdecadal variability: 1900–93. *Journal of climate* 10, 1004–1020.

TABLES

Table 1. Summary of data used in this thesis.

Study ID	Data Type	Source	Starting Year	Ending Year	Length of Record (Years)	N	Units
MEI	Climate Index	NOAA	1908	2017	110	1320	unitless
PDO	Climate Index	NOAA	1908	2017	110	1320	unitless
WTW	Precipitation	DWR	1908	2017	110	1320	mm
COR	Streamflow Discharge	USGS	1957	2017	61	732	m ³ /s
G001	Groundwater Levels	USGS	1947	1983	36	432	m
Inland/Coastal Groundwater Levels	Simulated Groundwater Levels	PVHM	1964	2014	51	612	m
Inland/Coastal Recharge	Simulated Recharge	PVHM	1963	2014	52	624	m ³
Inland/Coastal Pumping	Simulated Pumping	PVHM	1963	2014	52	624	m ³

Table 2. The percent variance of reconstructed components (RCs) attributed to the El Niño-Southern Oscillation (ENSO) and Pacific Decadal Oscillation (PDO) for all hydrologic datasets.

Dataset	Percent Variance	
	ENSO	PDO
Precipitation	6%	30%
Streamflow Discharge	10%	85%
<u>Simulated Recharge</u>		
<i>Coastal</i>	4%	93%
<i>Inland</i>	5%	92%
<u>Groundwater Pumping</u>		
<i>Coastal</i>	3%	90%
<i>Inland</i>	4%	82%
Observed Groundwater Levels	14%	85%
<u>Simulated Groundwater Levels</u>		
<i>Coastal</i>	2%	98%
<i>Inland</i>	1%	77%

Table 3. Results of the climate index to hydrologic inflows lag correlation. Correlations performed between El Niño-Southern Oscillation (ENSO) and Pacific Decadal Oscillation (PDO) composite reconstructed components (RCs) of climate indices and precipitation, streamflow discharge, and coastal and inland recharge. Minimum, maximum, and average correlation coefficients are reported in this table with their corresponding lag time in years. All

Index to Inflow	Minimum Correlation	Lag Time (years)	Maximum Correlation	Lag Time (years)	Average Correlation	Lag Time (years)
MEI - precipitation	0.07	0.08	0.31	1.1	0.22	1.1
MEI - streamflow discharge	0.06	1.3	0.29	0.17	0.21	0.63
MEI - coastal recharge	0.07	1.5	0.42	0.50	0.32	0.75
MEI - inland recharge	0.08	1.4	0.47	0.50	0.35	0.71
PDO - precipitation	0.06	0.33	0.12	1.9	0.10	1.9
PDO - streamflow discharge	0.08	4.0	0.60	1.0	0.45	2.0
PDO - coastal recharge	0.07	2.6	0.25	0.50	0.20	1.3
PDO - inland recharge	0.08	3.2	0.37	0.67	0.29	1.6

Table 4. Results of the climate index to hydrologic outflows lag correlation. Correlations performed between El Niño-Southern Oscillation (ENSO) and Pacific Decadal Oscillation (PDO) composite reconstructed components (RCs) of climate indices and simulated groundwater pumping. Minimum, maximum, and average correlation coefficients are reported in this table with their corresponding lag time in years.

Index to Outflow	Minimum Correlation	Lag Time (years)	Maximum Correlation	Lag Time (years)	Average Correlation	Lag Time (years)
MEI - coastal groundwater pumping	-0.08	1.0	-0.24	0.25	-0.20	0.50
MEI - inland groundwater pumping	-0.07	1.0	-0.21	0.25	-0.17	0.50
PDO - coastal groundwater pumping	-0.10	3.9	-0.25	0	-0.14	2.5
PDO - inland groundwater pumping	-0.06	2.0	-0.26	0	-0.16	0.95

Table 5. Results of the precipitation to inflows lag correlation. Correlations performed between El Niño-Southern Oscillation (ENSO) and Pacific Decadal Oscillation (PDO) composite reconstructed components (RCs) of precipitation to streamflow discharge and groundwater recharge. Minimum, maximum, and average correlation coefficients are reported in this table with their corresponding lag time in years.

Precipitation to Inflow	Minimum Correlation	Lag Time (years)	Maximum Correlation	Lag Time (years)	Average Correlation	Lag Time (years)
<u>ENSO-composite</u>						
Precipitation - streamflow discharge	0.10	1.1	0.80	0	0.53	0.54
Precipitation - coastal recharge	0.10	1.0	0.73	0	0.47	0.50
Precipitation - inland recharge	0.13	0.90	0.74	0	0.49	0.45
<u>PDO-composite</u>						
Precipitation - streamflow discharge	0.07	4.3	0.87	0.67	0.64	2.1
Precipitation - coastal recharge	0.08	3.6	0.71	0.20	0.50	1.8
Precipitation - inland recharge	0.08	3.5	0.8	0.20	0.60	1.8

Table 6. Results of the inflows to outflows lag correlation. Correlations performed between El Niño-Southern Oscillation (ENSO) and Pacific Decadal Oscillation (PDO) composite reconstructed components (RCs) of inflows to groundwater pumping. Minimum, maximum, and average correlation coefficients are reported in this table with their corresponding lag time in years.

Outflows to Groundwater Levels	Minimum Correlation	Lag Time (years)	Maximum Correlation	Lag Time (years)	Average Correlation	Lag Time (years)
<u>ENSO-composite</u>						
Coastal groundwater pumping - observed groundwater levels	-0.07	1.7	-0.41	0	-0.25	0.88
Inland groundwater pumping - observed groundwater levels	-0.07	1.7	-0.41	0	-0.23	0.83
Coastal groundwater pumping - coastal groundwater levels	-0.11	1.5	-0.57	0.58	-0.42	0.75
Inland groundwater pumping - inland groundwater levels	-0.08	0.25	-0.37	1.3	-0.26	1.4
<u>PDO-composite</u>						
Coastal groundwater pumping - observed groundwater levels	-0.09	4.4	-0.36	5.0	-0.22	4.7
Inland groundwater pumping - observed groundwater levels	-0.08	2.1	-0.37	0.80	-0.29	.01
Coastal groundwater pumping - coastal groundwater levels	-0.07	4.3	-0.9	0	-0.60	2.1
Inland groundwater pumping - inland groundwater levels	-0.43	5.0	-0.73	1.9	-0.64	2.5

Table 7. Results of the climate index to groundwater levels lag correlation. Correlations performed between El Niño-Southern Oscillation (ENSO) and Pacific Decadal Oscillation (PDO) composite reconstructed components (RCs) of climate indices to observed and simulated groundwater levels. Minimum, maximum, and average correlation coefficients are reported in this table with their corresponding lag time in years. (*) Despite using 60 months as the maximum forward lag limit, the lag correlation between the PDO Index and observed groundwater levels did not result in a positive correlation coefficient for the first 60 lags. The threshold was extended in this case and the first statistically significant correlation coefficient was reported in this table.

Index to Groundwater Level	Minimum Correlation	Lag Time (years)	Maximum Correlation	Lag Time (years)	Average Correlation	Lag Time (years)
MEI - observed groundwater levels	0.07	2.2	0.44	3.3	0.28	3.3
MEI - coastal groundwater levels	0.08	2.5	0.42	1.3	0.29	1.5
MEI - inland groundwater levels	0.06	0.67	0.48	1.67	0.32	1.7
PDO - observed groundwater levels	0.06*	7.5*	0.06*	7.5*	0.06*	7.5*
PDO - coastal groundwater levels	0.07	4.8	0.44	0.83	0.31	2.4
PDO - inland groundwater levels	0.23	5.0	0.46	2.4	0.38	2.5

Table 8. Results of inflows to groundwater levels lag correlation. Correlations performed between El Niño-Southern Oscillation (ENSO) and Pacific Decadal Oscillation (PDO) composite reconstructed components (RCs) of inflows to observed and simulated groundwater levels. Minimum, maximum, and average correlation coefficients are reported in this table with their corresponding lag time in years.

Inflows to Groundwater Levels	Minimum Correlation	Lag Time (years)	Maximum Correlation	Lag Time (years)	Average Correlation	Lag Time (years)
<u>ENSO-composite</u>						
Precipitation - observed groundwater levels	0.07	2.2	0.43	3.3	0.31	3.1
Precipitation - coastal groundwater levels	0.10	1.8	0.72	0.67	0.53	0.92
Precipitation - inland groundwater levels	0.07	2.0	0.67	0.92	0.47	1.0
Streamflow discharge - observed groundwater levels	0.08	1.2	0.25	0.25	0.19	0.58
Streamflow discharge - coastal groundwater levels	0.08	1.8	0.67	0.58	0.47	0.90
Streamflow discharge - inland groundwater levels	0.10	2.0	0.62	0.92	0.43	1.0
Coastal Recharge - observed groundwater levels	0.08	1.7	0.51	0.50	0.36	0.83
Inland Recharge - observed groundwater levels	0.09	1.6	0.52	0.50	0.37	0.80
Coastal Recharge - coastal groundwater levels	0.10	1.75	0.64	0.75	0.46	0.88
Inland Recharge - inland groundwater levels	0.13	1.9	0.68	1.0	0.46	0.96

Table 8. (Cont.)

Inflows to Groundwater Levels	Minimum Correlation	Lag Time (years)	Maximum Correlation	Lag Time (years)	Average Correlation	Lag Time (years)
<u>PDO-composite</u>						
Precipitation - observed groundwater levels	0.10	0	0.65	2.7	0.50	2.5
Precipitation - coastal groundwater levels	0.25	0	0.50	2.8	0.43	2.5
Precipitation - inland groundwater levels	0.10	0	0.59	3.3	0.45	2.5
Streamflow discharge - observed groundwater levels	0.10	0	0.67	4.8	0.52	2.5
Streamflow discharge - coastal groundwater levels	0.38	0	0.63	3.0	0.56	2.5
Streamflow discharge - inland groundwater levels	0.32	0	0.77	3.3	0.65	2.5
Coastal Recharge - observed groundwater levels	0.37	5.0	0.87	1.9	0.71	2.5
Inland Recharge - observed groundwater levels	0.25	0	0.82	2.7	0.68	2.5
Coastal Recharge - coastal groundwater levels	0.09	0	0.64	4.6	0.47	2.5
Inland Recharge - inland groundwater levels	0.06	0	0.63	5.0	0.44	2.9

Table 9. Results of the outflows to groundwater levels lag correlation. Correlations performed between El Niño-Southern Oscillation (ENSO) and Pacific Decadal Oscillation (PDO) composite reconstructed components (RCs) of groundwater pumping to observed and simulated groundwater levels. Minimum, maximum, and average correlation coefficients are reported in this table with their corresponding lag time in years.

Outflows to Groundwater Levels	Minimum Correlation	Lag Time (years)	Maximum Correlation	Lag Time (years)	Average Correlation	Lag Time (years)
<u>ENSO-composite</u>						
Coastal groundwater pumping - observed groundwater levels	-0.07	1.7	-0.41	0	-0.25	0.88
Inland groundwater pumping - observed groundwater levels	-0.07	1.7	-0.41	0	-0.23	0.83
Coastal groundwater pumping - coastal groundwater levels	-0.11	1.5	-0.57	0.58	-0.42	0.75
Inland groundwater pumping - inland groundwater levels	-0.08	0.25	-0.37	1.3	-0.26	1.4
<u>PDO-composite</u>						
Coastal groundwater pumping - observed groundwater levels	-0.09	4.4	-0.36	5.0	-0.22	4.7
Inland groundwater pumping - observed groundwater levels	-0.08	2.1	-0.37	0.8	-0.29	1.0
Coastal groundwater pumping - coastal groundwater levels	-0.07	4.3	-0.90	0	-0.60	2.1
Inland groundwater pumping - inland groundwater levels	-0.43	5.0	-0.73	1.9	-0.64	2.5

FIGURES

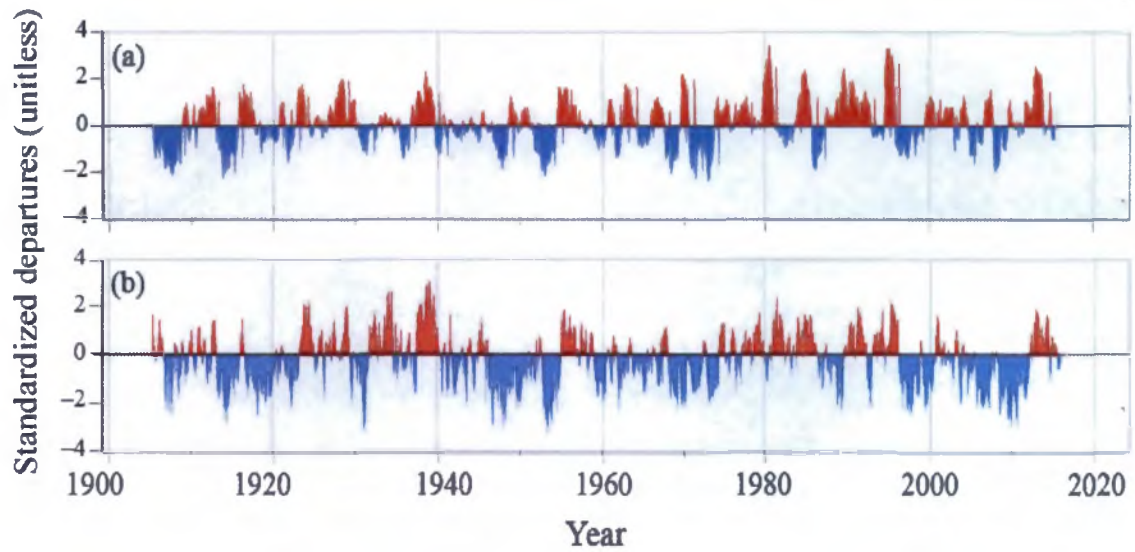


Figure 1. The (a) Multivariate ENSO Index on a monthly timescale, and the (b) Pacific Decadal Oscillation Index on a monthly timescale (NOAA, 2018).

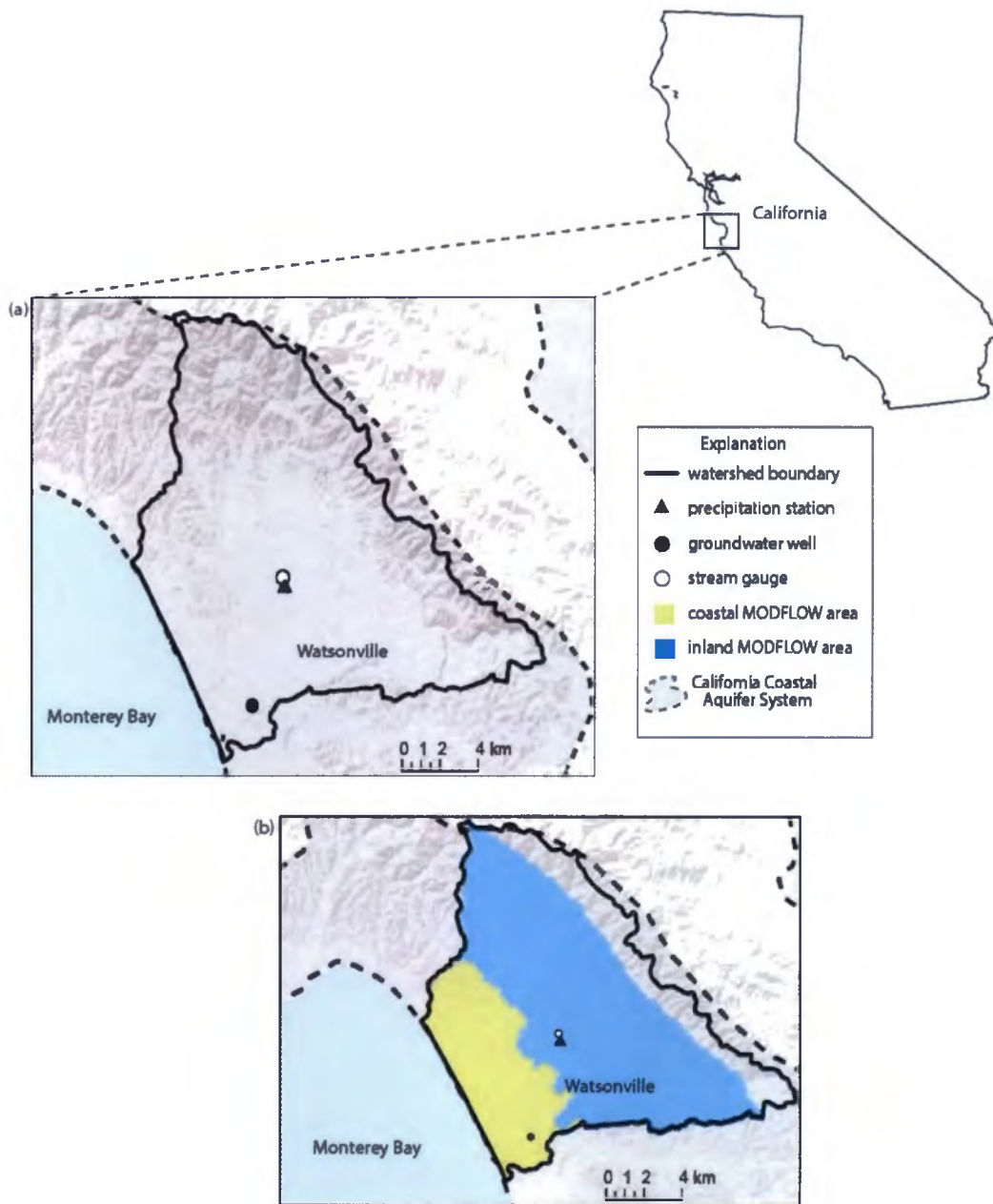


Figure 2. Map of Pajaro Valley, CA with (a) stations for observed data and (b) area of simulated data

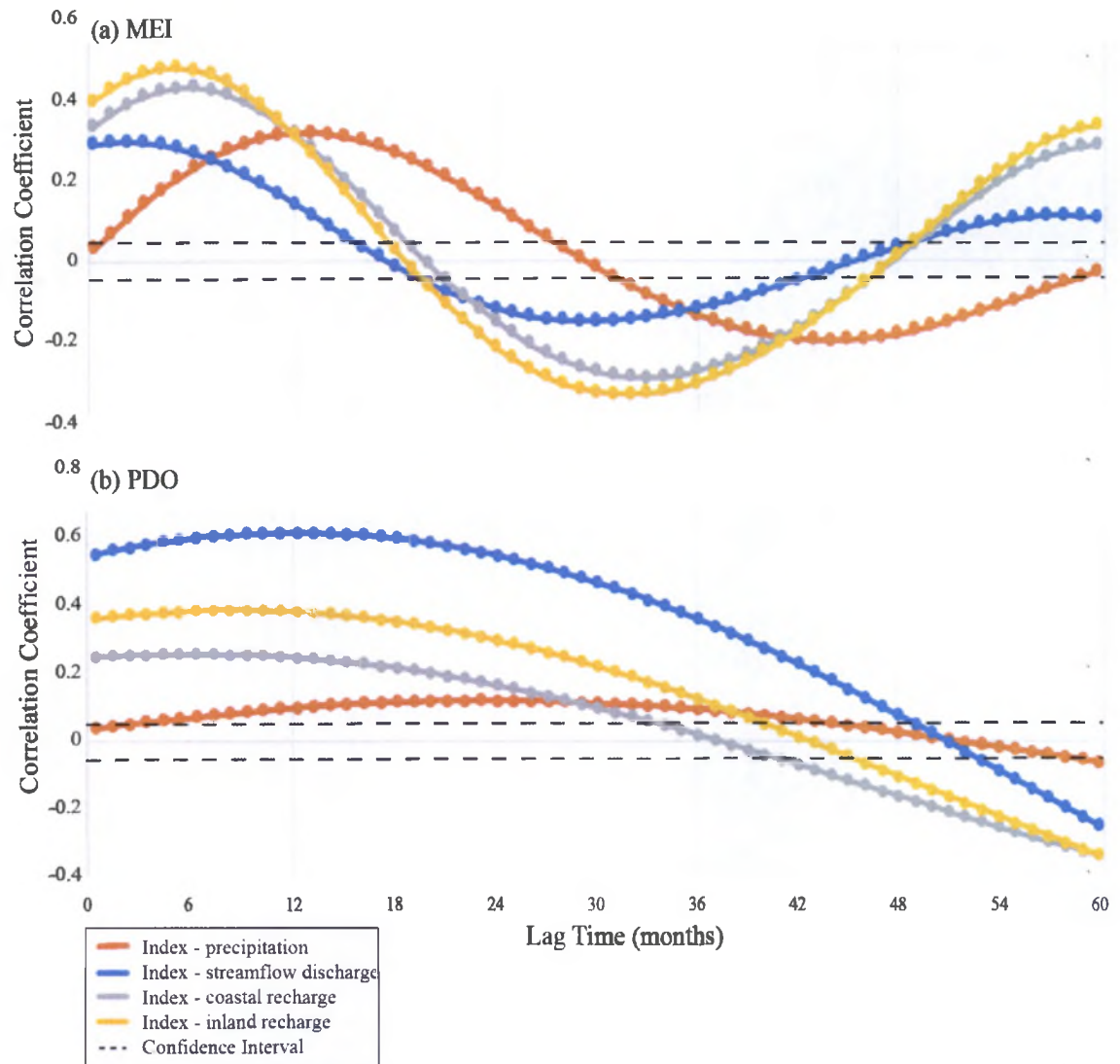


Figure 3. Lag correlation plot of the (a) MEI and (b) PDO to hydrologic inflows. Correlation coefficients above the confidence interval are statistically significant.

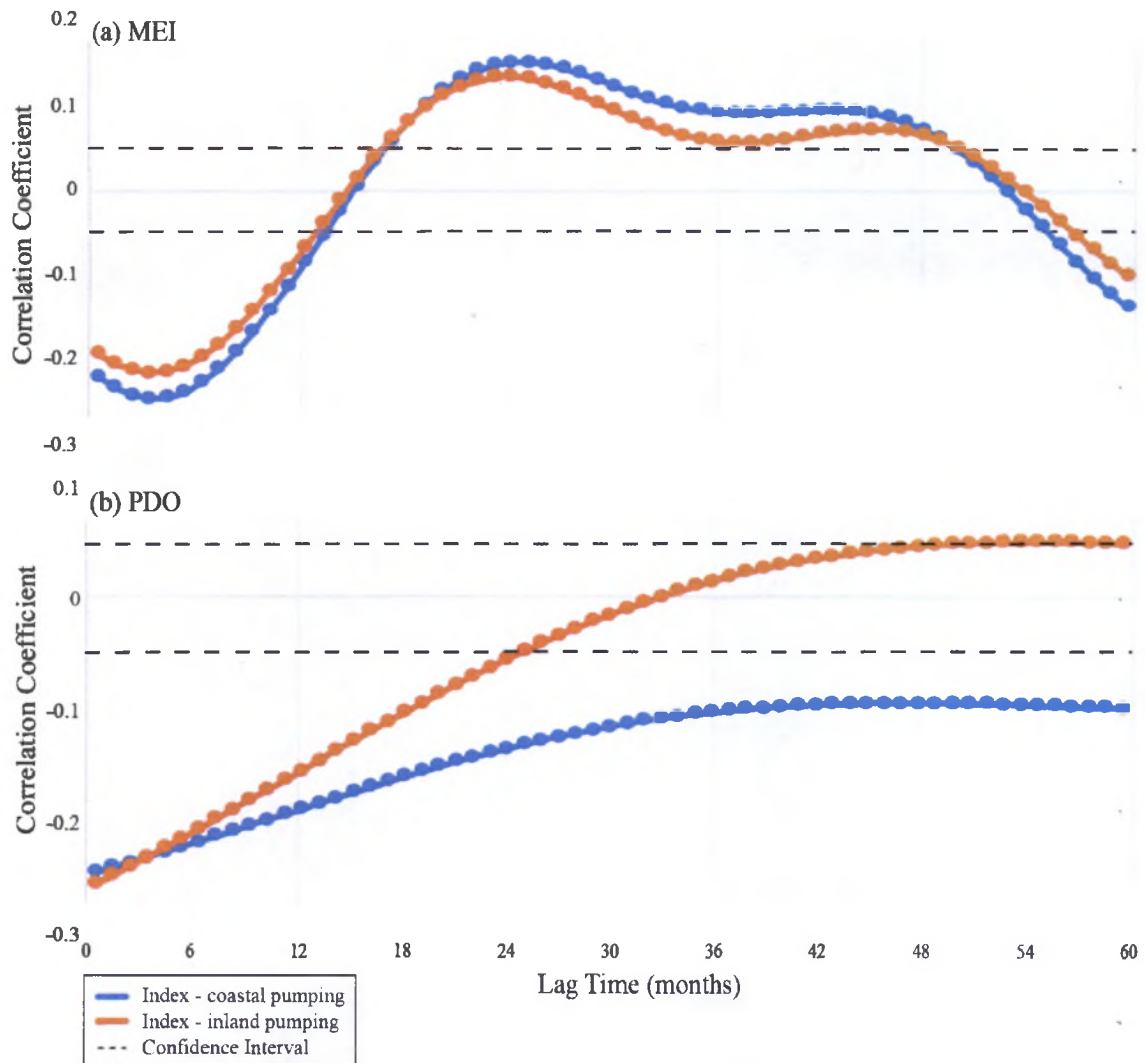


Figure 4. Lag correlation plot of the (a) MEI and (b) PDO to hydrologic outflows. Correlation coefficients above the confidence interval are statistically significant.

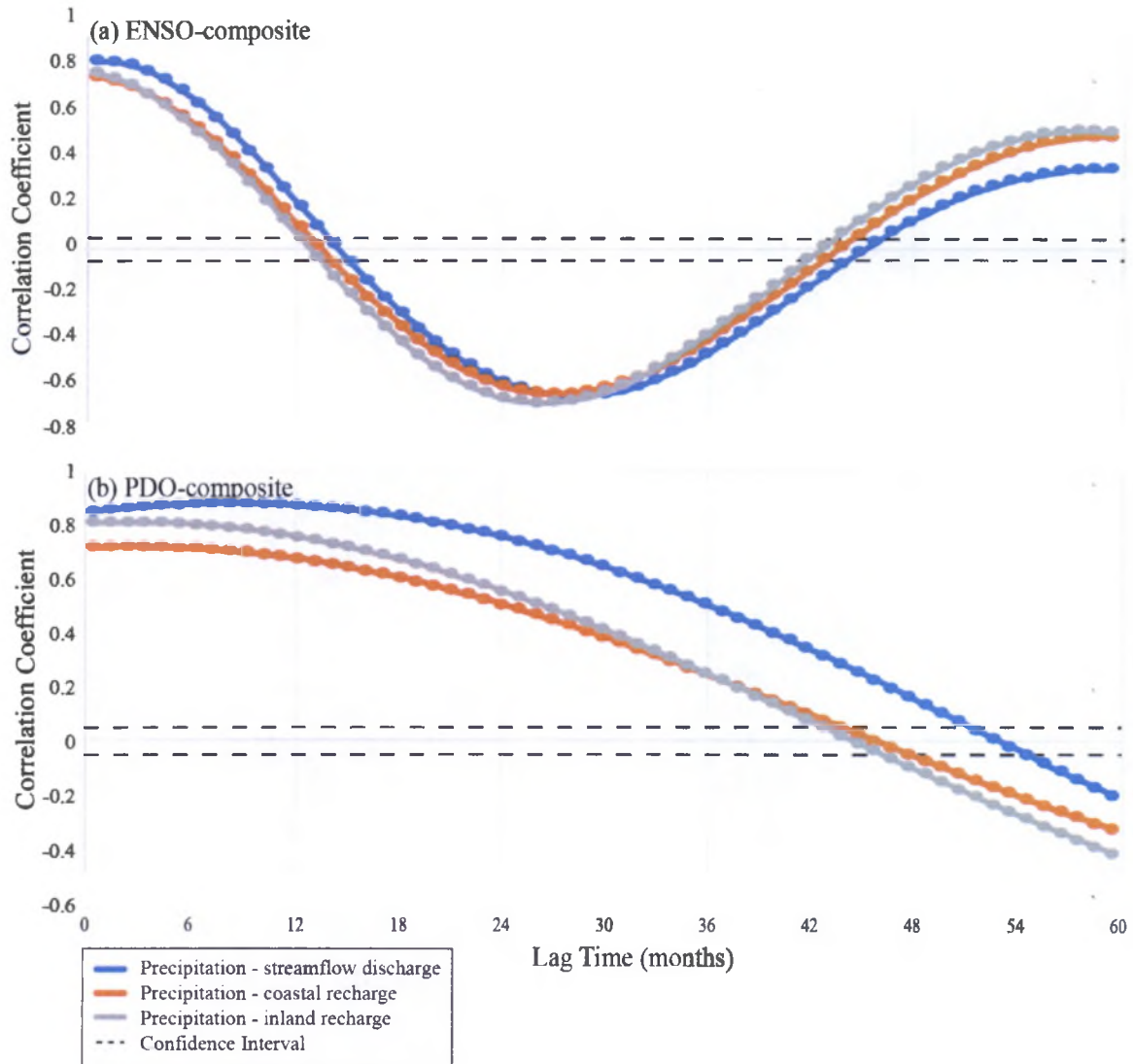


Figure 5. Lag correlation plot of precipitation to inflows for (a) ENSO-composite and (b) PDO-composite RCs. Correlation coefficients above the confidence interval are statistically significant.

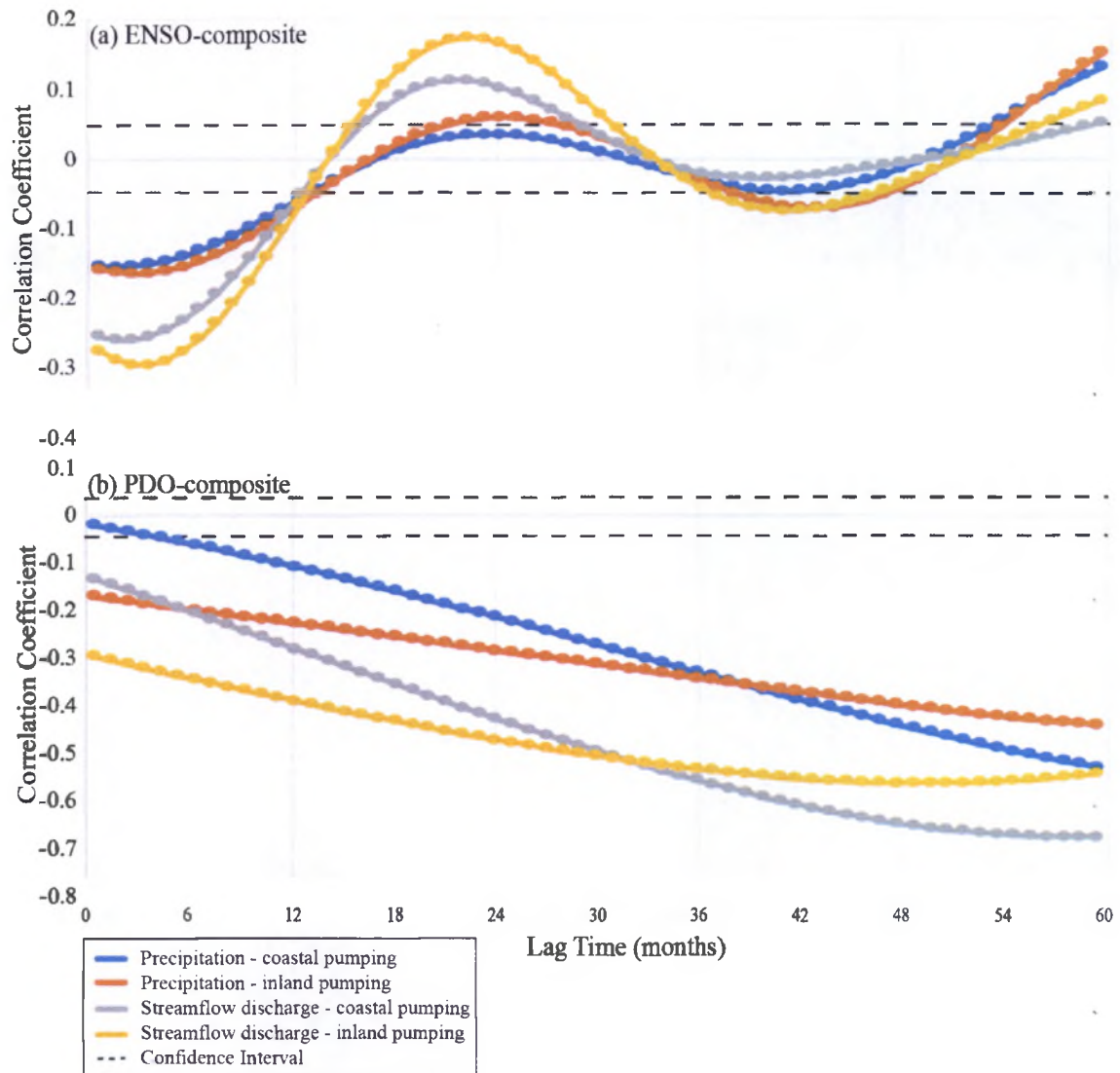


Figure 6. Lag correlation plot of inflows to outflows for (a) ENSO-composite and (b) PDO-composite RCs. Correlation coefficients above the confidence interval are statistically significant.

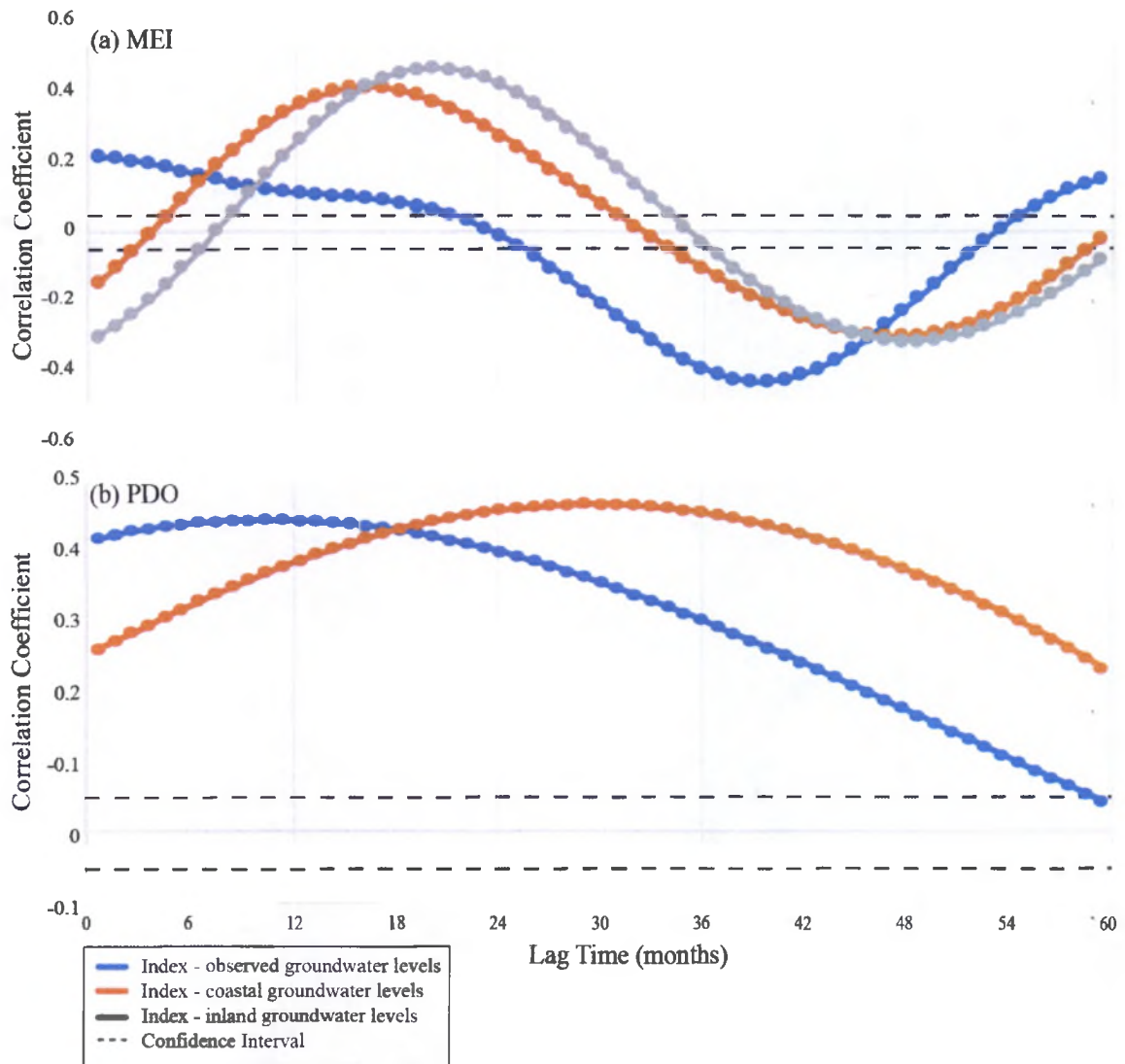


Figure 7. Lag correlation plot of the (a) MEI and (b) PDO to observed and simulated groundwater levels. Correlation coefficients above the confidence interval are statistically significant.

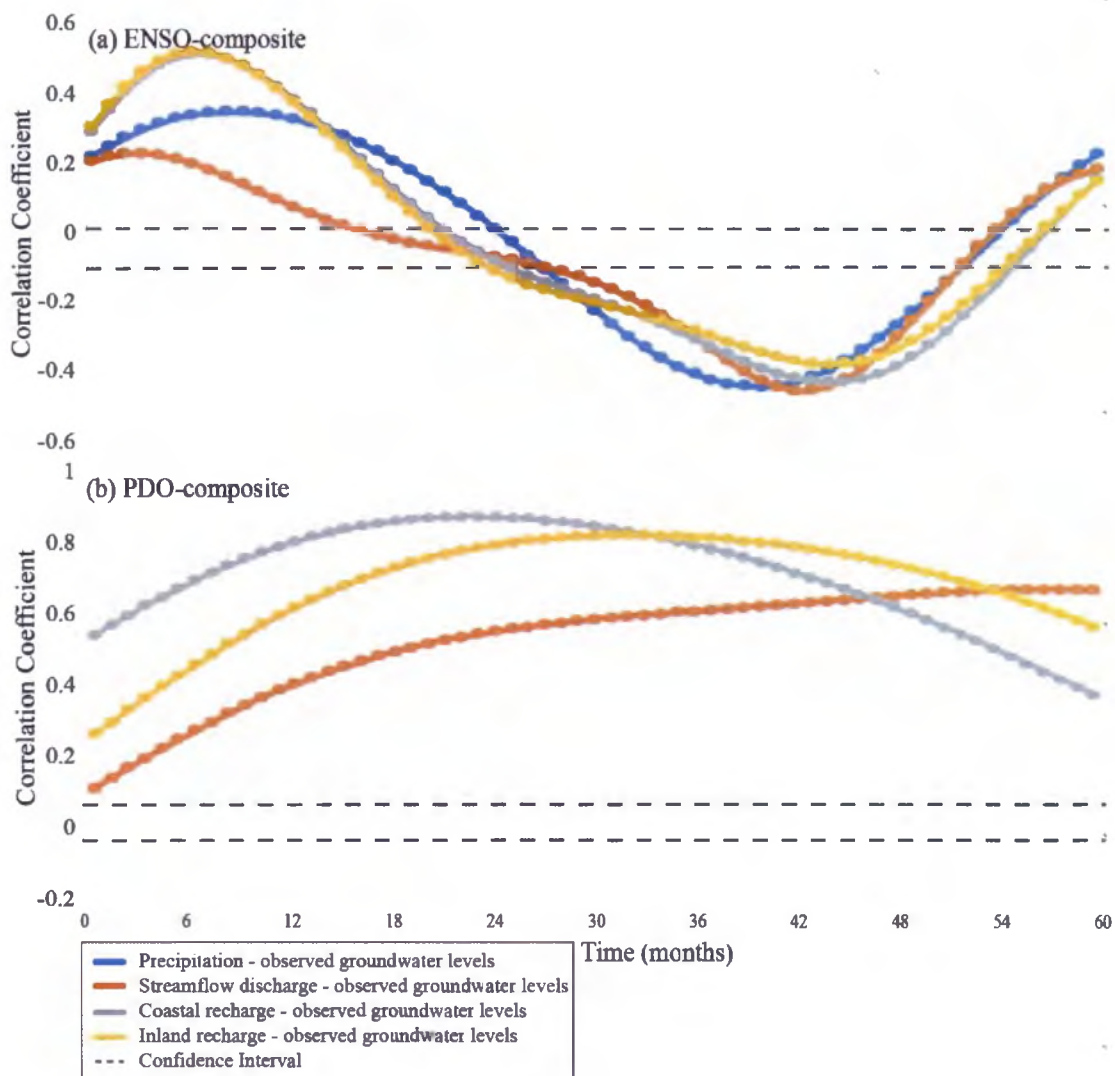


Figure 8. Lag correlation plot of hydrologic inflows to observed groundwater levels for (a) ENSO-composite and (b) PDO-composite RCs. Correlation coefficients above the confidence interval are statistically significant.

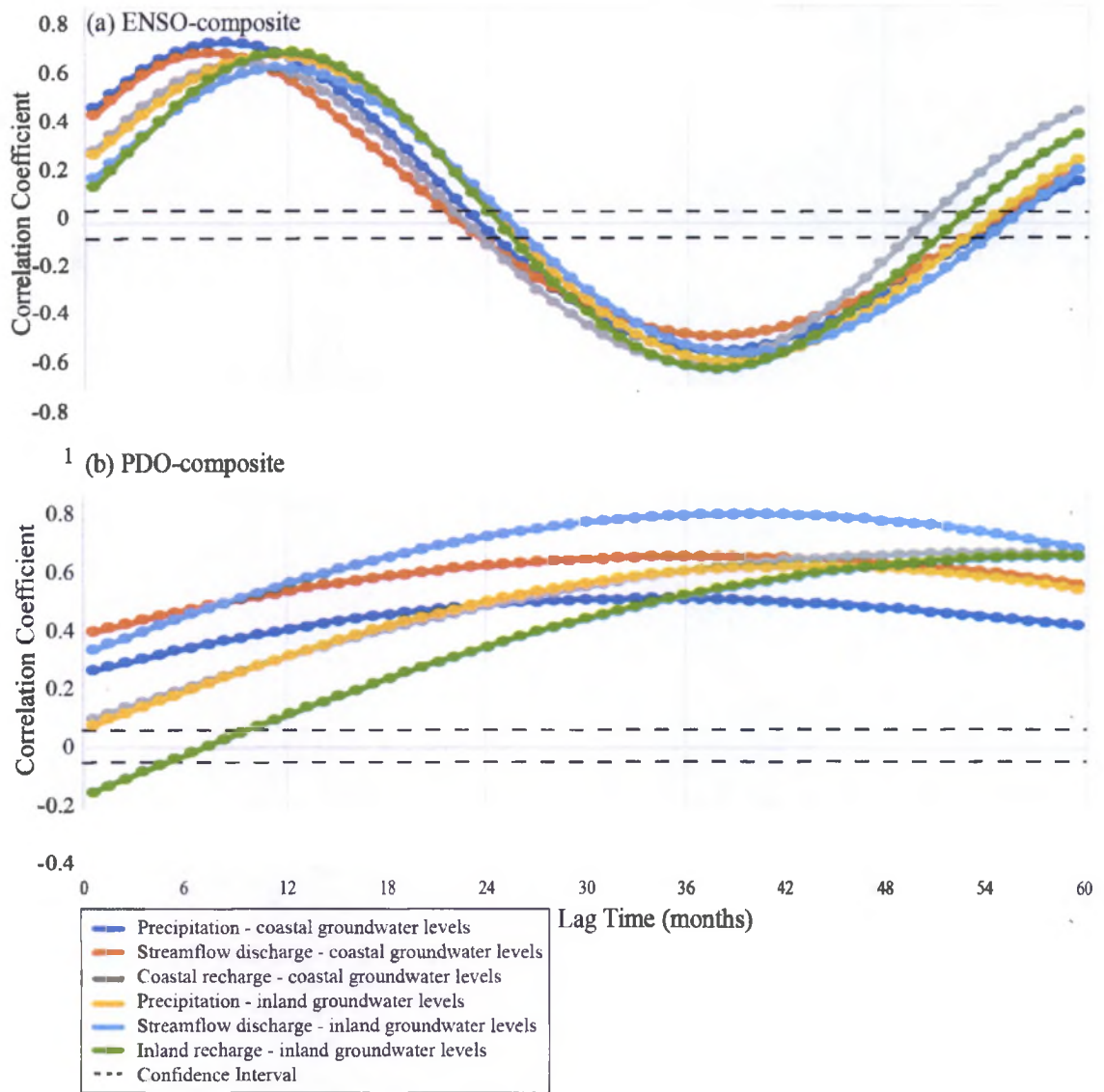


Figure 9. Lag correlation plots of hydrologic inflows to simulated groundwater levels for (a) ENSO-composite and (b) PDO-composite RCs. Correlation coefficients above the confidence interval are statistically significant.

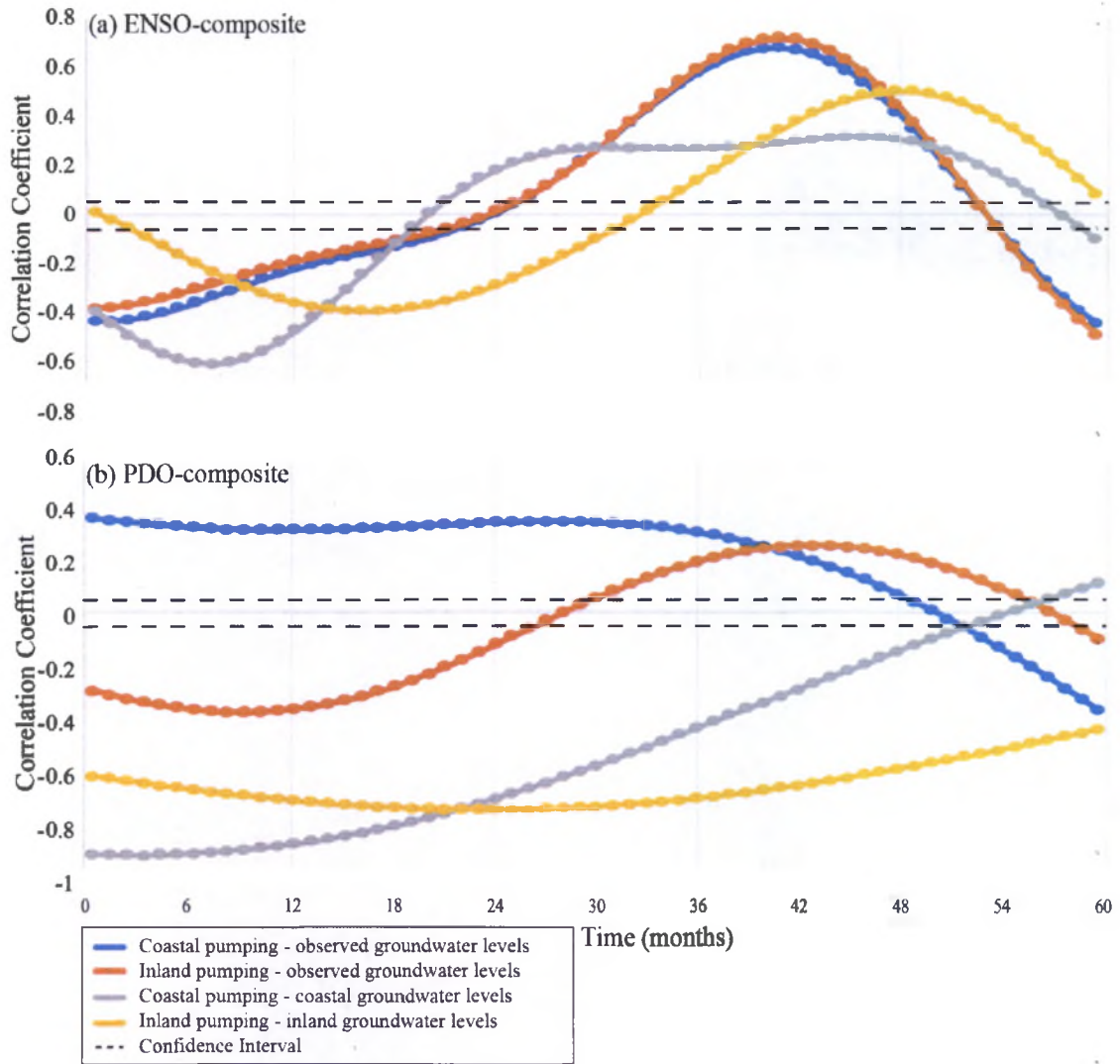


Figure 10. Lag correlation plot of hydrologic outflows to observed and simulated groundwater levels for (a) ENSO-composite and (b) PDO-composite RCs. Correlation coefficients above the confidence interval are statistically significant.

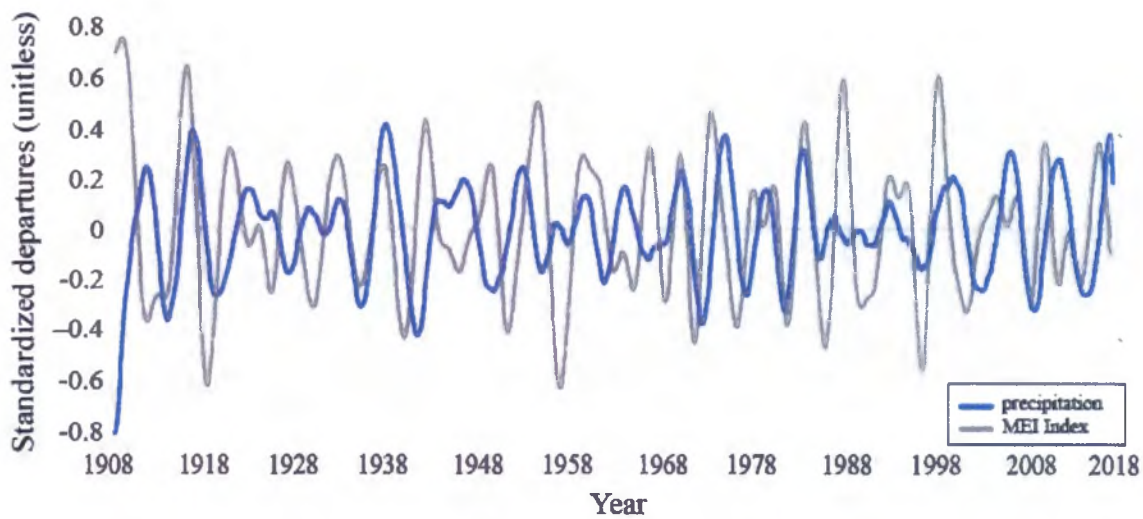


Figure 11. Timeseries of ENSO-composite RCs of precipitation plotted with the MEI Index.

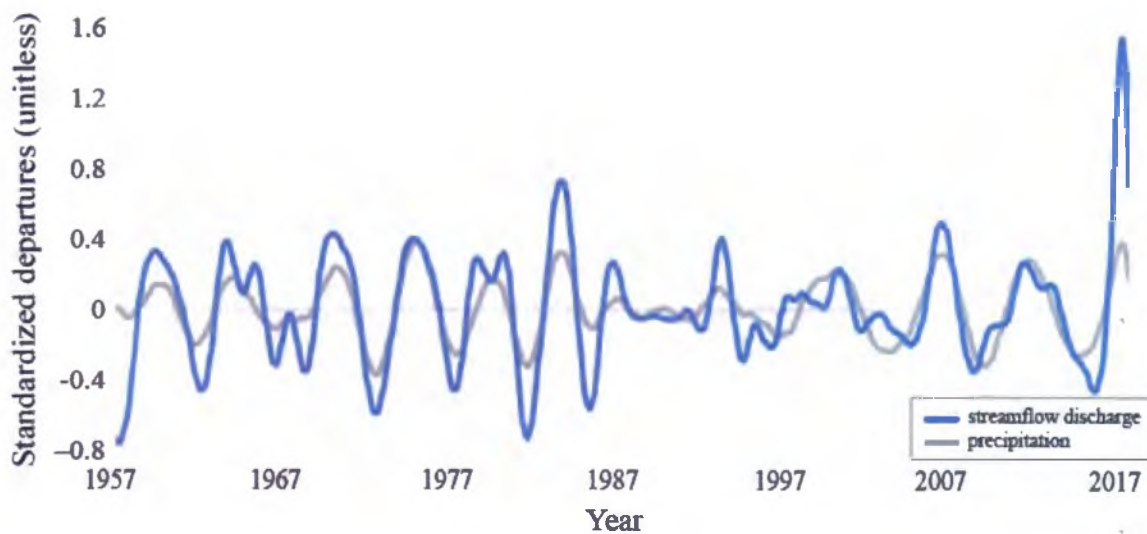


Figure 12. Timeseries of ENSO-composite RCs of precipitation and streamflow discharge.

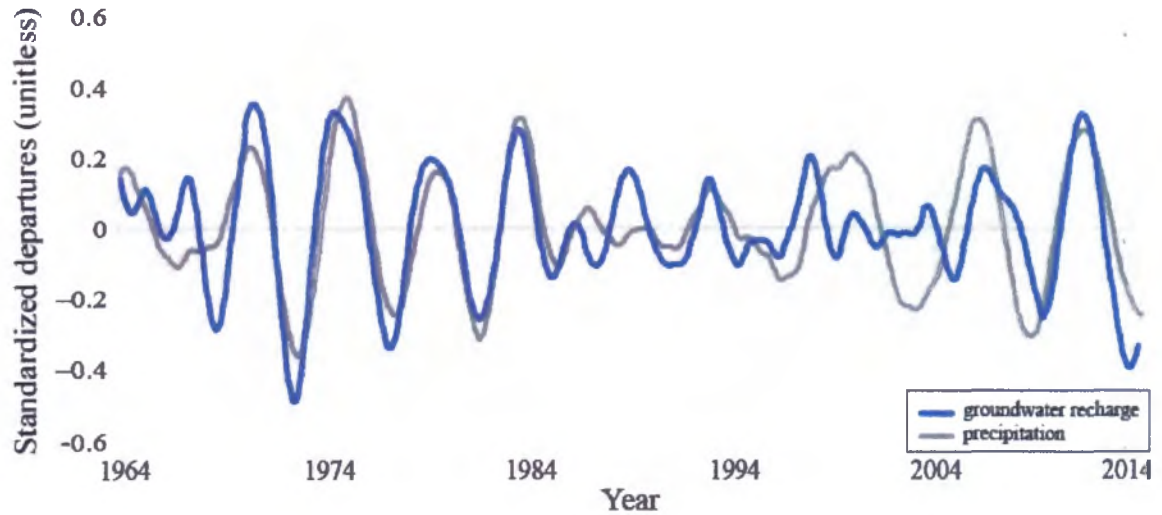


Figure 13. Timeseries of ENSO-composite RCs of precipitation and simulated groundwater recharge.

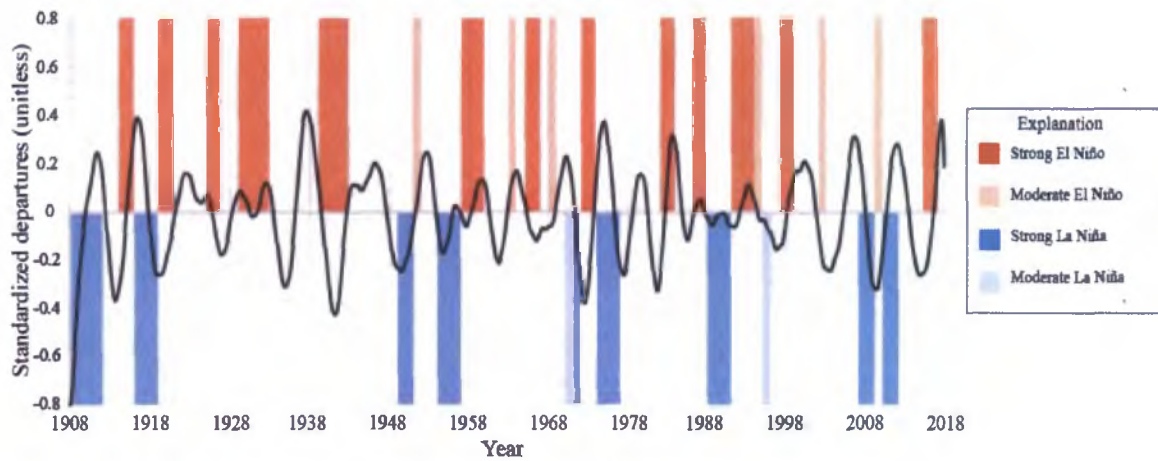


Figure 14. Exported ENSO-composite RCs within the precipitation timeseries are plotted with phases of strong to moderate El Niño and La Niña events (NOAA, ESRL, 2019).

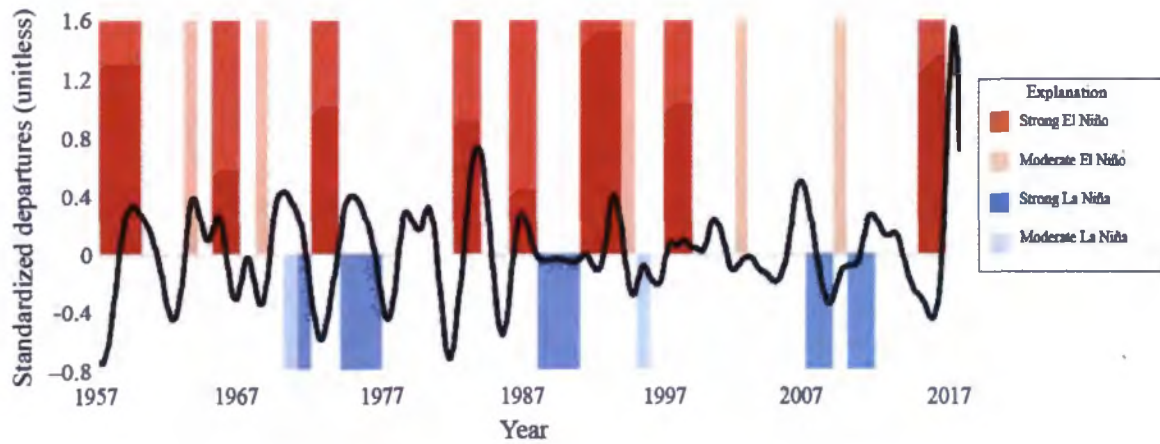


Figure 15. Exported ENSO-composite RCs within the streamflow discharge timeseries are plotted with phases of strong to moderate El Niño and La Niña events (NOAA, ESRL, 2019).

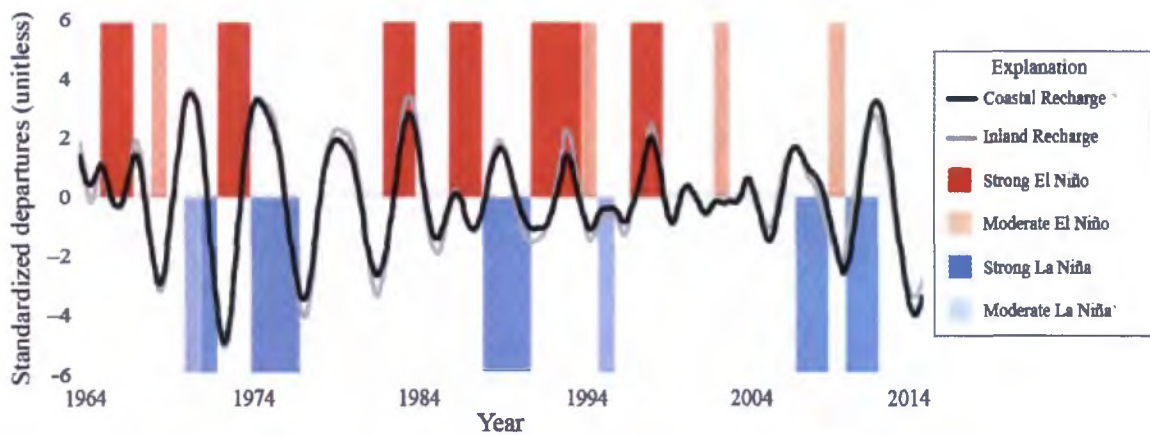


Figure 16. Exported ENSO-composite RCs within the simulated groundwater recharge timeseries are plotted with phases of strong to moderate El Niño and La Niña events (NOAA, ESRL, 2019).

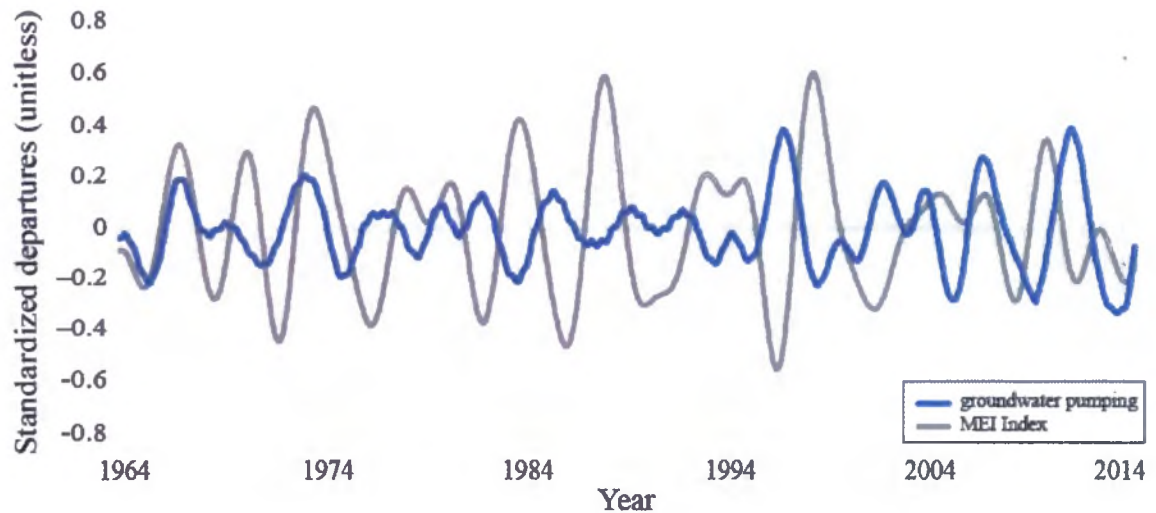


Figure 17. Timeseries of ENSO-composite simulated groundwater pumping plotted with the MEI Index.

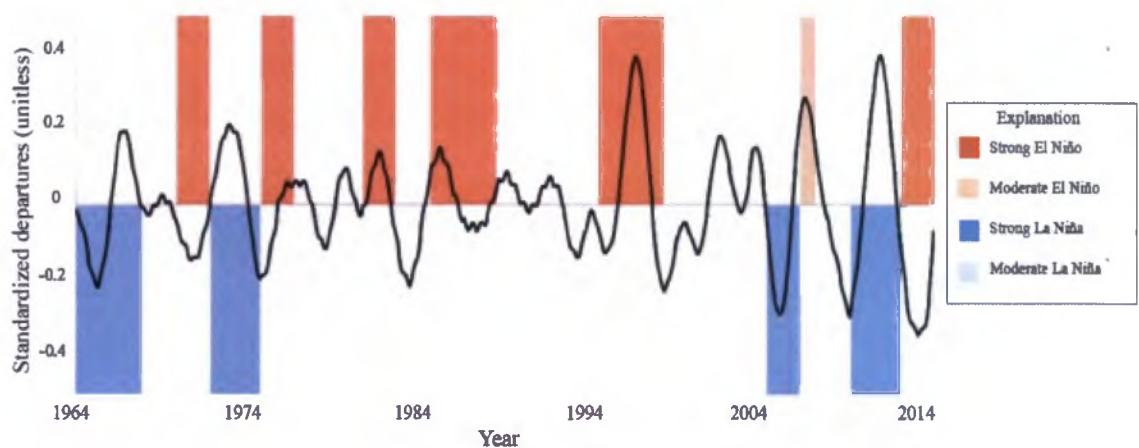


Figure 18. Exported ENSO-composite RCs of simulated groundwater pumping volume are plotted with phases of strong to moderate El Niño and La Niña events (NOAA, ESRL, 2019). Coastal and inland pumping data were averaged for the purpose of clarity.

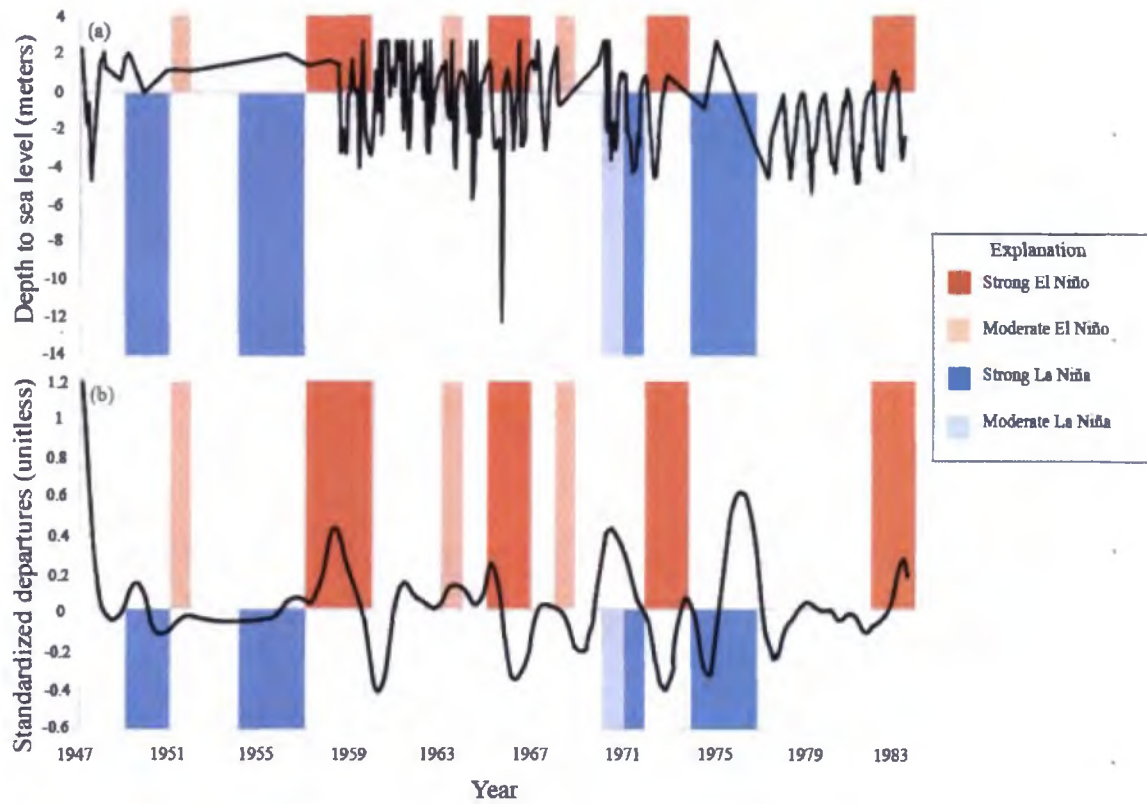


Figure 19. The (a) raw observed groundwater levels and (b) exported ENSO-composite RCs of observed groundwater levels are plotted with phases of strong to moderate El Niño and La Niña events (NOAA, ESRL, 2019).

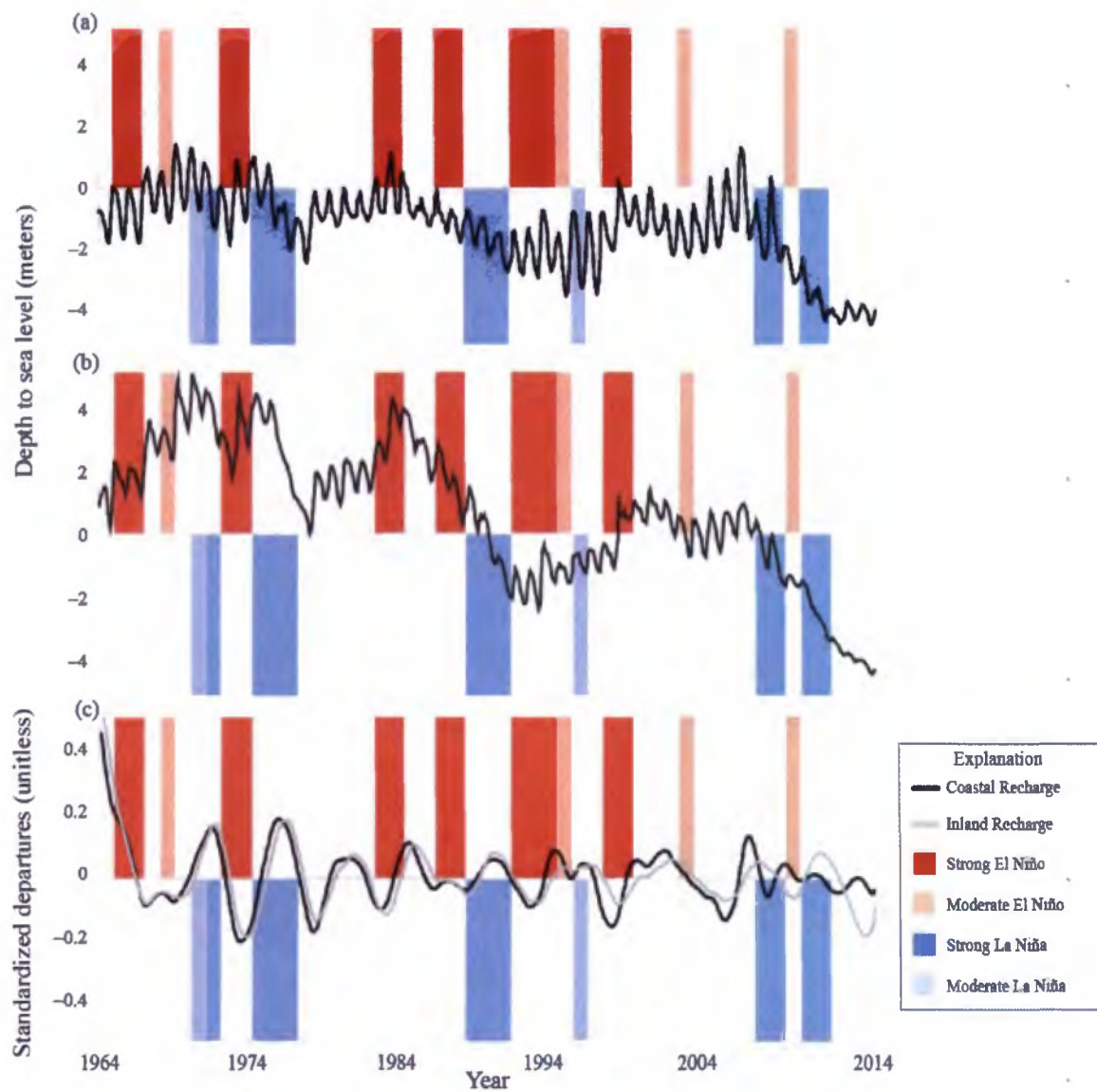


Figure 20. The (a) raw coastal, (b) raw inland, and the (c) exported ENSO-composite RCs of simulated groundwater levels are plotted with phases of strong to moderate El Niño and La Niña events (NOAA, ESRL, 2019).

APPENDIX

Appendix A. Results of the Singular Spectrum Analysis. Bolded rows denote components that were used to create ENSO and PDO-composite RCs.

ID	Reconstructed Component (RC)	Period	Frequency	Power	Variance	Error of Power	Error of Variance	Period (Years)	CV Matches
MEI	1	660.00	0.00	84.77	0.65	3.30	0.03	55.00	
	2	220.00	0.00	28.80	0.22	1.12	0.01	18.33	
	3	110.00	0.01	5.78	0.04	0.22	0.00	9.17	
	4	77.65	0.01	3.88	0.03	0.15	0.00	6.47	ENSO
	5	62.86	0.02	3.30	0.03	0.13	0.00	5.24	ENSO
	6	45.52	0.02	1.73	0.01	0.07	0.00	3.79	ENSO
	7	42.58	0.02	1.07	0.01	0.04	0.00	3.55	ENSO
	8	42.58	0.02	0.58	0.00	0.02	0.00	3.55	ENSO
	9	34.74	0.03	0.30	0.00	0.01	0.00	2.89	ENSO
	10	29.33	0.03	0.23	0.00	0.01	0.00	2.44	ENSO

Appendix B. Results of the Singular Spectrum Analysis (Cont.)

ID	Reconstructed Component (RC)	Period	Frequency	Power	Variance	Error of Power	Error of Variance	Period (Years)	CV Matches
PDO	1	984.00	0.00	125.45	0.59	4.00	0.02	82.00	
	2	492.00	0.00	66.09	0.31	2.11	0.01	41.00	
	3	218.67	0.00	10.19	0.05	0.32	0.00	18.22	PDO
	4	115.76	0.01	4.12	0.02	0.13	0.00	9.65	
	5	109.33	0.01	1.78	0.01	0.06	0.00	9.11	
	6	67.86	0.01	1.35	0.01	0.04	0.00	5.66	
	7	67.86	0.01	1.19	0.01	0.04	0.00	5.66	
	8	56.23	0.02	0.51	0.00	0.02	0.00	4.69	
	9	51.79	0.02	0.29	0.00	0.01	0.00	4.32	
	10	45.77	0.02	0.26	0.00	0.01	0.00	3.81	
WTW	1	660.00	0.00	66.73	0.60	2.60	0.02	55.00	
	2	440.00	0.00	26.28	0.24	1.02	0.01	36.67	PDO
	3	146.67	0.01	7.29	0.07	0.28	0.00	12.22	PDO
	4	82.50	0.01	3.22	0.03	0.13	0.00	6.88	ENSO
	5	62.86	0.02	1.71	0.02	0.07	0.00	5.24	ENSO
	6	12.00	0.08	1.13	0.01	0.04	0.00	1.00	
	7	12.00	0.08	1.08	0.01	0.04	0.00	1.00	
	8	55.00	0.02	0.83	0.01	0.03	0.00	4.58	ENSO
	9	47.14	0.02	0.36	0.00	0.01	0.00	3.93	ENSO
	10	40.00	0.03	0.21	0.00	0.01	0.00	3.33	ENSO
G001	1	222.00	0.00	19.64	0.85	1.32	0.06	18.50	PDO
	2	74.00	0.01	2.86	0.12	0.19	0.01	6.17	ENSO
	3	27.75	0.04	0.30	0.01	0.02	0.00	2.31	ENSO
	4	12.00	0.08	0.18	0.01	0.01	0.00	1.00	
	5	12.00	0.08	0.15	0.01	0.01	0.00	1.00	
	6	9.45	0.11	0.03	0.00	0.00	0.00	0.79	
	7	8.38	0.12	0.01	0.00	0.00	0.00	0.70	
	8	6.43	0.16	0.01	0.00	0.00	0.00	0.54	
	9	6.00	0.17	0.01	0.00	0.00	0.00	0.50	
	10	5.10	0.20	0.00	0.00	0.00	0.00	0.43	

Appendix B. Results of the Singular Spectrum Analysis (Cont.)

ID	Reconstructed Component (RC)	Period	Frequency	Power	Variance	Error of Power	Error of Variance	Period (Years)	CV Matches
COR	1	183.00	0.01	40.11	0.54	2.10	0.03	15.25	PDO
	2	146.40	0.01	23.46	0.31	1.23	0.02	12.20	PDO
	3	56.31	0.02	3.85	0.05	0.20	0.00	4.69	ENSO
	4	56.31	0.02	2.27	0.03	0.12	0.00	4.69	ENSO
	5	40.67	0.02	0.86	0.01	0.05	0.00	3.39	ENSO
	6	12.00	0.08	0.74	0.01	0.04	0.00	1.00	
	7	12.00	0.08	0.73	0.01	0.04	0.00	1.00	
	8	26.14	0.04	0.41	0.01	0.02	0.00	2.18	ENSO
	9	26.14	0.04	0.36	0.00	0.02	0.00	2.18	ENSO
	10	22.18	0.05	0.31	0.00	0.02	0.00	1.85	
Inland Pumping	1	312.00	0.00	36.91	0.60	2.09	0.03	26.00	PDO
	2	208.00	0.00	13.74	0.22	0.78	0.01	17.33	PDO
	3	12.24	0.08	4.06	0.07	0.23	0.00	1.02	
	4	12.24	0.08	3.84	0.06	0.22	0.00	1.02	
	5	62.40	0.02	1.54	0.03	0.09	0.00	5.20	ENSO
	6	39.00	0.03	0.53	0.01	0.03	0.00	3.25	ENSO
	7	29.71	0.03	0.21	0.00	0.01	0.00	2.48	ENSO
	8	6.12	0.16	0.14	0.00	0.01	0.00	0.51	
	9	6.12	0.16	0.14	0.00	0.01	0.00	0.51	
	10	27.13	0.04	0.11	0.00	0.01	0.00	2.26	ENSO
Coastal Pumping	1	312.00	0.00	40.36	0.65	2.29	0.04	26.00	PDO
	2	208.00	0.00	15.68	0.25	0.89	0.01	17.33	PDO
	3	12.24	0.08	1.92	0.03	0.11	0.00	1.02	
	4	12.24	0.08	1.82	0.03	0.10	0.00	1.02	
	5	62.40	0.02	1.26	0.02	0.07	0.00	5.20	ENSO
	6	41.60	0.02	0.35	0.01	0.02	0.00	3.47	ENSO
	7	31.20	0.03	0.15	0.00	0.01	0.00	2.60	ENSO
	8	29.71	0.03	0.08	0.00	0.00	0.00	2.48	ENSO
	9	6.12	0.16	0.07	0.00	0.00	0.00	0.51	
	10	6.12	0.16	0.07	0.00	0.00	0.00	0.51	

Appendix B. Results of the Singular Spectrum Analysis (Cont.)

ID	Reconstructed Component (RC)	Period	Frequency	Power	Variance	Error of Power	Error of Variance	Period (Years)	CV Matches
Coastal Groundwater Levels	1	306.00	0.00	40.18	0.73	2.30	0.04	25.50	PDO
	2	204.00	0.00	13.67	0.25	0.78	0.01	17.00	PDO
	3	61.20	0.02	0.67	0.01	0.04	0.00	5.10	ENSO
	4	47.08	0.02	0.15	0.00	0.01	0.00	3.92	ENSO
	5	12.00	0.08	0.07	0.00	0.00	0.00	1.00	
	6	12.00	0.08	0.06	0.00	0.00	0.00	1.00	
	7	30.60	0.03	0.04	0.00	0.00	0.00	2.55	ENSO
	8	25.50	0.04	0.02	0.00	0.00	0.00	2.13	ENSO
	9	21.86	0.05	0.01	0.00	0.00	0.00	1.82	
	10	19.74	0.05	0.00	0.00	0.00	0.00	1.65	
Inland Groundwater Levels	1	306.00	0.00	45.55	0.77	2.60	0.04	25.50	PDO
	2	122.40	0.01	12.95	0.22	0.74	0.01	10.20	
	3	61.20	0.02	0.66	0.01	0.04	0.00	5.10	ENSO
	4	47.08	0.02	0.12	0.00	0.01	0.00	3.92	ENSO
	5	30.60	0.03	0.02	0.00	0.00	0.00	2.55	ENSO
	6	12.00	0.08	0.01	0.00	0.00	0.00	1.00	
	7	12.00	0.08	0.01	0.00	0.00	0.00	1.00	
	8	25.50	0.04	0.01	0.00	0.00	0.00	2.13	ENSO
	9	21.86	0.05	0.00	0.00	0.00	0.00	1.82	
	10	19.74	0.05	0.00	0.00	0.00	0.00	1.65	
Inland Recharge	1	312.00	0.00	45.11	0.68	2.55	0.04	26.00	PDO
	2	156.00	0.01	15.70	0.24	0.89	0.01	13.00	PDO
	3	56.73	0.02	2.09	0.03	0.12	0.00	4.73	ENSO
	4	56.73	0.02	0.92	0.01	0.05	0.00	4.73	ENSO
	5	12.24	0.08	0.35	0.01	0.02	0.00	1.02	
	6	12.24	0.08	0.34	0.01	0.02	0.00	1.02	
	7	27.13	0.04	0.33	0.01	0.02	0.00	2.26	ENSO
	8	22.29	0.04	0.27	0.00	0.02	0.00	1.86	
	9	20.80	0.05	0.23	0.00	0.01	0.00	1.73	
	10	16.42	0.06	0.15	0.00	0.01	0.00	1.37	

Appendix B. Results of the Singular Spectrum Analysis (Cont.)

ID	Reconstructed Component (RC)	Period	Frequency	Power	Variance	Error of Power	Error of Variance	Period (Years)	CV Matches
Coastal Recharge	1	312.00	0.00	46.97	0.73	2.66	0.04	26.00	PDO
	2	156.00	0.01	13.08	0.20	0.74	0.01	13.00	PDO
	3	56.73	0.02	1.82	0.03	0.10	0.00	4.73	ENSO
	4	56.73	0.02	0.76	0.01	0.04	0.00	4.73	ENSO
	5	28.36	0.04	0.26	0.00	0.01	0.00	2.36	ENSO
	6	12.24	0.08	0.25	0.00	0.01	0.00	1.02	
	7	12.24	0.08	0.25	0.00	0.01	0.00	1.02	
	8	22.29	0.04	0.21	0.00	0.01	0.00	1.86	
	9	20.80	0.05	0.18	0.00	0.01	0.00	1.73	
	10	16.42	0.06	0.12	0.00	0.01	0.00	1.37	